Chapter 4
Practical Aspects

The quality of NMR spectra is critically dependent on numerous factors, among which are the condition of the instrument at the time the data are collected, the homogeneity of the magnetic field, the type of experiments chosen, how the data are acquired and subsequently processed, etc. In this chapter, practical aspects related to the experiments are discussed in detail.

Key questions to be addressed in the current chapter include the following:

1. How is a probe tuned correctly?
2. What is a simple and correct way to do shimming?
3. How are transmitter (or observe) hard pulses calibrated?
4. How are decoupler (nonobserve) hard pulses calibrated?
5. How are the pulse lengths of decoupling calibrated?
6. What is the procedure to calibrate selective pulses?
7. How are the offset frequencies of the transmitter and decoupler calibrated and how often are they calibrated?
8. How can off-resonance pulses ($^{13}C'$, $^{13}C^{\alpha}$, $^{13}C^{\alpha,\beta}$) be calibrated?
9. How is the temperature calibration of a probe done?
10. What is the decoupling efficiency of different decoupling methods?
11. How is pulsed field gradient used to remove unwanted magnetization?
12. What are coherence and coherence transfer?
13. What is the coherence transfer pathway?
14. How are they selected by phase cycling or gradient methods?
15. What are the common water suppression techniques?
16. What are the advantage and drawbacks of the techniques?
17. How are the water suppression experiments set up?
18. How is a 2D (or 3D, 4D) experiment formed and what is the intrinsic difference between 1D and multidimensional experiments?
19. What are the typical procedures used to set up an experiment?
20. What is the typical procedure for processing data?

Q. Teng, *Structural Biology: Practical NMR Applications*,
DOI 10.1007/978-1-4614-3964-6_4,

4.1 Tuning the Probe

The general procedure for setting up routine NMR experiments is described in the flow chart of Fig. 4.1. Tuning probe is the initial step before NMR data can be acquired. As discussed in Chap. 1, in order to move the equilibrium magnetization away from the magnetic field direction, an oscillating magnetic field B_1 generated by an RF pulse during NMR experiments, is needed to interact with the nuclei at Larmor frequency. In order to efficiently use the RF energy, the probe must be tuned to the carrier frequency (center frequency of the spectrum) for the sample to be measured and the impedance of the probe must be matched to the instrument impedance of 50 Ω at resonance (Chap. 2). Incorrect tuning or matching of the probe will cause an increased 90° pulse length and decreased sensitivity of detection.

Probe tuning and matching are carried out by adjusting the capacitors of the coil circuits in the probe. Probe tuning refers to the adjustment of both the probe resonance frequency to the carrier frequency, and the probe impedance to match 50 Ω. A common triple-resonance solution NMR probe consists of two coils, of which the inner is double-tuned to ^{1}H and ^{2}H and the outer to ^{13}C and ^{15}N for a HCN probe or to ^{13}C and other heteronuclei over a wide range for an HCX probe, in which X represents a heteronucleus in the broadband range. Usually, each channel has a pair of adjustable capacitors, one for tuning and the other for matching. Some of the probes have auto-matched ^{15}N and ^{13}C channels, in which only tuning capacitors need to be adjusted. There are no adjustable matching capacitors for heteronuclear channels in this kind of probe. A typical procedure for tuning the probe involves turning the rods (or sliding bars) of the two adjustable capacitors alternatively and detecting the change of probe resonance frequency and impedance after setting up the carrier frequency for each channel being tuned.

Tuning should always be performed first for the nucleus with the lowest Larmor frequency, then for those with higher resonance frequency because the higher frequency is more sensitive to small changes in capacitance of the probe circuits, which can be caused by tuning neighboring channels. For instance, the ^{15}N channel

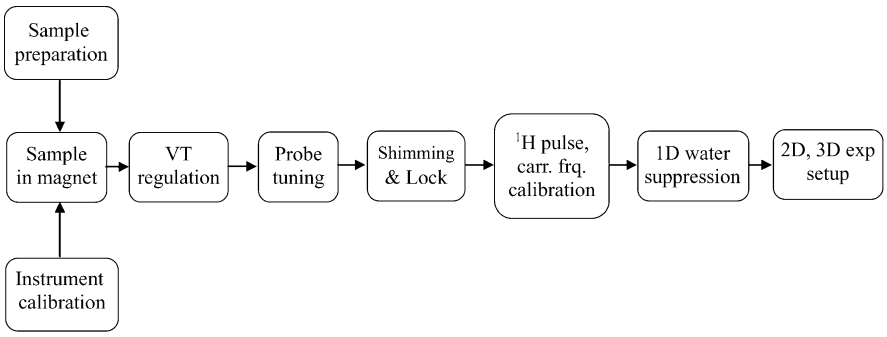

Fig. 4.1 Flowchart of a typical procedure for NMR experiment setup. The instrument must be properly calibrated before the experiment can be performed (see text for details). Each of the steps is discussed in the current chapter except sample preparation (previous chapter) and setup of 3D experiments (following chapter)

is tuned first, then ^{13}C, and the ^{1}H channel is tuned last. In high field spectrometers the dielectric field of sample solvents is sufficiently high to influence the capacitance of probe circuits, resulting in a shift of probe resonance frequency when changing samples. Therefore, the probe must be tuned every time a sample is placed in the magnet. Since the circuits are temperature dependent, the probe must also be tuned after it reaches the selected temperature when the temperature is regulated.

There are two common methods used in probe tuning and matching: detecting the reflection power or detecting the resonance frequency of the probe during tuning and matching. Both methods are standard capabilities of NMR spectrometers. The reflection power method observes the RF power reflected by the probe and is more frequently used in routine tuning. When the spectrometer is in the tuning mode, RF pulses at the carrier frequency of the nucleus being tuned are delivered to the probe channel. This tuning method aims to minimize the amount of power being reflected by the probe. At the resonance condition with the input RF pulses, the probe circuit holds most of the power it receives. Thus, when a probe is well tuned, it reflects a minimum portion of the power being delivered to it and uses the RF power more efficiently. Consequently, a 90° pulse length is shorter for a given amount of RF power, compared to a mistuned probe.

The reflection power tuning method uses a directional coupler and a voltage meter to display the portion of the RF power reflected by the probe after a RF pulse with a specific frequency is sent to the probe. The RF pulses are set to the carrier frequency of the nuclei being tuned. Usually, the repetition rate is short, which is about five 20 μs pulses per second. The receiver does not need to be on during probe tuning (use a large number of steady-state scans or dummy scans). Most spectrometers setup the tuning parameters and start pulsing automatically, when in probe tuning mode. Practically, the capacitance of the probe circuits is adjusted by first turning the tuning capacitor (or sliding a bar) in a direction to reduce the amount of reflected RF power, until the reflection reaches a minimum. Keep turning the capacitor in the same direction, which makes the reflected power pass the minimum and increase by just a small amount. The next step is to adjust the matching capacitor in a direction so that the reflected power is back to a new minimum. If the new minimum is smaller than the previous one, keep turning the matching capacitor to pass the minimum by a small amount. If the new minimum is higher than the previous one, start with the adjustment of the tuning capacitor again but in the opposite direction so that a lower minimum can be found. Then, the above procedure is repeated by alternatively adjusting tuning and matching capacitors until the reflection power is best minimized. Usually, the ^{1}H channel of the probe can be tuned so well that the reading of power reflected from probe is zero. Normally, the reflection power reading for the heteronuclear channel is a little higher but the 90° pulse lengths are still in the range of the specifications (<40 μs for ^{15}N, <15 μs for ^{13}C).

Tuning using a spectral analyzer and an RF bridge to display the resonance frequency of the probe is another common method, referred as the wobbler method. The majority of NMR spectrometers have the capability to do the wobbler tuning as a standard feature (for instance, “qtune” on Agilent instruments and “wobb” on Bruker instruments). The basic procedure is the same as the reflection method except that the resonance frequency of the probe is monitored when adjusting the

capacitors. The first step is to adjust the tuning capacitor so that the dip on the display moves from one side of the setup frequency to the other, approximately by 50 kHz. Adjusting the matching capacitor then makes the dip pass the setup frequency back to the original side. If the dip of the signal is lower, repeat the above process until it reaches a minimum. If the dip is higher than the initial value, change the direction. The depth of the dip indicates how well the impedance of the probe circuit matches to 50 Ω. The best tuning position is indicated by the lowest dip of the probe resonance frequency at the setup frequency.

The probe should be tuned every time the sample is changed, as noted above, especially for those with different solvents or salt concentrations because the dielectric property of the solvents affects the capacitance of probe circuits. However, the tuning of heteronuclear channels is not sensitive to different samples provided the sample does not contain a large amount of salts because the probe coil for heteronuclear channels is the outer coil. Thus, the tuning of ^{15}N and ^{13}C channels does not change much from sample to sample. It should also be noted that the correct way to tune the probe is without any filters attached because probe tuning aims to tune the resonance frequency of the probe. Filters are not integrated parts of the probe circuits and have their own resonance frequencies, which may alter the power fed into them. Therefore, the measurement of the reflected power should be performed directly at the probe output, rather than at any later stage.

4.2 Shimming and Locking

Because superior homogeneity of the magnetic field across the sample volume is necessary in order to obtain a sharp line shape in NMR spectra, the static magnetic field, B_0, must be perfected by adjusting the current to a series of coils inside the magnet (more details in Chap. 2). The process is called "shimming" and the coils called shimming coils. The number of the coils can be as many as 40 sets, which produce a magnetic field across the sample volume. Manually shimming the magnet is a rather complicated process and very time-consuming. It is difficult to manually shim higher order z shims (z shims only alter the magnetic field along the z direction and are also called spinning shims) such as z^5, z^6 or z^7 because they are dependent on each other, which means that a change in one of them alters the others. Shimming nonspinning shims (xy shims that only change the field in the xy plane) is relatively easy because most of them are independent of the others. Fortunately, gradient technology has been used in magnet shimming, called gradient shimming, and greatly reduces the amount of work in shimming. Gradient shimming of spinning shims requires a z gradient capability of the instrument, whereas gradient shimming of nonspinning or xy shims requires x and y gradients. Usually, solution NMR instruments do not have x, y pulsed field gradients (PFGs), and, hence, gradient shimming normally applies only on z shims.

Under normal operating conditions, all NMR magnets have a constantly fluctuating field strength due to the environment. The magnetic field is stabilized

by a mini spectrometer operated at the ^{2}H frequency, which continuously observes the ^{2}H signal frequency through the dedicated lock channel to maintain a stable magnetic field. If the observed ^{2}H frequency deviates from the set value, the spectrometer changes the magnetic field strength in the opposite way through a coil inside the magnet to compensate for the fluctuation. This process is called "lock" and is carried out in real time. Four parameters are important to have correct operation of locking: lock field (also known as z_0 field), which is the ^{2}H resonance frequency of the solvent (or the offset of the ^{2}H lock frequency); lock power, which controls the ^{2}H RF power used to generate the ^{2}H signal; lock gain, which is used to amplify the signal received by lock receiver; and lock phase, which sets the correct dispersion phase of the ^{2}H signal used to monitor the deviation of the ^{2}H lock frequency caused by the B_0 magnetic field fluctuation. They should all be optimized for lock. The common procedure is to adjust z_0 first to be on resonance for the ^{2}H solvent. After locking on the ^{2}H, the lock power is adjusted to the highest possible level without saturating the lock signal. Saturation is the point at which the lock level is decreased when lock power increases. Then the lock power is slightly reduced to surely avoid the saturation (e.g., by 10%). The lock gain is adjusted to bring the lock level to 80%, which is the most sensitive level. Finally, the lock phase is optimized to maximize the lock level.

The lock level is monitored during manual shimming, which is the observation of the ^{2}H signal. The better the homogeneity of the field is, the higher the lock level, provided the lock phase is correctly adjusted. The FID of water may also be used to monitor the quality of shimming. When using the lock level for shimming, the lock phase must be properly adjusted because a poorly phased lock signal distorts the maximum intensity of the signal, which is used to monitor the homogeneity of the magnetic field. A distorted lock intensity (lock level) may not represent the field homogeneity linearly.

If the shimming is off significantly after changing samples, it is important to first adjust the z shims while spinning the sample. If z gradient auto shimming will be used, only z_1–z_3 need to be shimmed manually. The usual procedure is to adjust z_1 and z_2 alternatively to obtain a lock level as high as possible. Then z_3 needs to be optimized before z_1 and z_2 are revisited. The above procedure is repeated until the maximum lock level is reached. After initial adjustment on the z shims, the nonspinning shims must be shimmed without spinning the sample. The procedure usually is the following order:

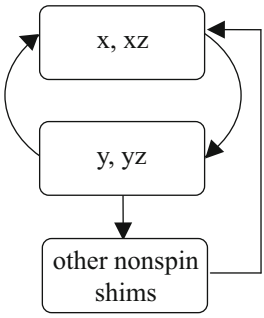

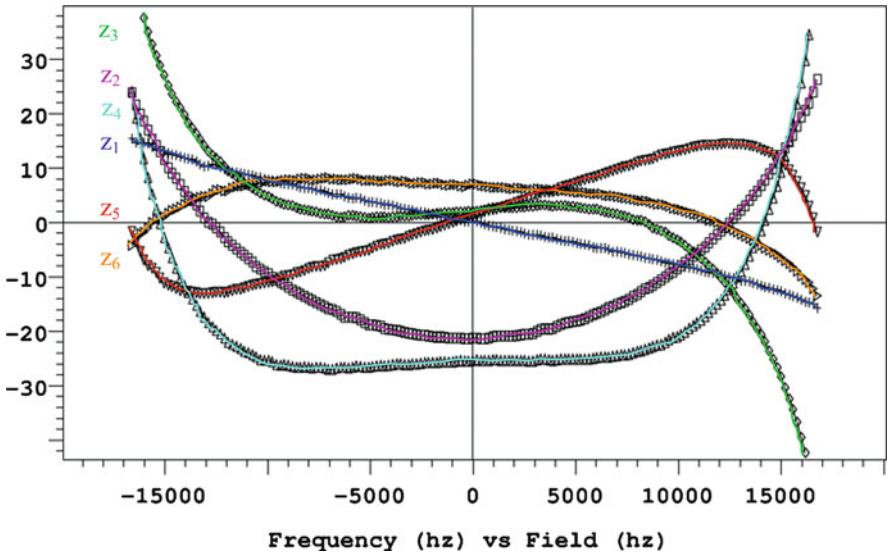

Fig. 4.2 Profiles of shimming gradients z_1–z_6 indicated by the shim map. The x-axis corresponds to the sample position along the z axis of the NMR tube with the zero frequency corresponding to the center of the sample. For this plot, the negative frequency is from the sample in the bottom of the NMR tube

where x and xz are shimmed first, then y and yz to optimize the lock level. The steps are repeated until the lock level does not increase. The rest of the nonspinning shims are checked one by one. If any of them changes the lock level, shims x, xz, y, and yz need to be checked again.

Gradient shimming, which provides rapid automatic optimization of room-temperature shims, is one of the profound applications of PFGs. It not only provides reliable shimming results on high-order z shims (and nonspinning shims) within a minute, which otherwise would take many hours if shimming manually, but also allows one to shim on nuclei besides ^{2}H, such as ^{1}H. It is critically useful for samples without ^{2}H solvent. For instance, a methanol sample is commonly used for calibration of variable temperature control. Without ^{1}H gradient shimming, it is impossible to shim on the sample because it does not contain ^{2}H solvent. It is usually done by shimming a deuterated methanol sample with the same volume as the calibration sample. By using ^{1}H gradient shimming, one can shim on the actual calibration sample (more in the temperature calibration section). Gradient shimming requires PFG capability (PFG amplifier and probe), which is a standard feature of NMR instruments for biological research, although it can be done by homospoil gradient through the z_1 room-temperature shim coil. It is a standard practice to always apply z gradient shimming on all NMR samples. It involves generating a gradient shim map first (an example is shown in Fig. 4.2), shimming z_1–z_4 using the map and then z_1–z_6. The shim map can be repeatedly used for different samples with the same probe provided the sample volume is approximately the same as the sample used to generate the map. Nonspinning shims must

be optimized before the shim map is generated. By no means, is what has been described above the only way to perform shimming. There are different shimming methods available in different laboratories. However, in our hands, the above procedure has not failed.

"Deuterium lock frequency" and "lock field" are two terms that are sometimes easily confused. The lock frequency is the instrument's ^{2}H frequency at the magnetic field, whereas the lock field—as mentioned earlier—is the ^{2}H resonance frequency of the solvent. The function of the z_0 field (or lock field) is twofold. Different solvents have different ^{2}H resonance frequencies. The slightly different ^{2}H frequencies are adjusted by changing the z_0 field. The other situation that requires changing z_0 is when the magnetic field drifts. On the other hand, the lock frequency is unchanged as long as z_0 is adjustable, that is, z_0 is not out of range. Therefore, even if the magnetic field drifts (field strength decreases due to loss of current in the SC solenoid of the magnet), a constant field strength is maintained by changing the value of the z_0 field. In other words, the offset frequencies (see below), the chemical shift reference, and other field dependent qualities are unchanged when the instrument lock frequency is unchanged even if the magnetic field strength drifts as the magnet ages because the drifted field is compensated for through the adjustment of z_0.

4.3 Instrument Calibrations

4.3.1 Calibration of Variable Temperature

For each probe, the actual temperature vs. the setting value must be calibrated before data are collected for real samples. A typical method for temperature calibration over the range of −20 to 50°C is to observe the chemical shift difference ($\Delta\delta$ in ppm) between the two peaks of 100% methanol. The empirical expression in the relationship of the observed $\Delta\delta$ with temperature is given by:

$$T(^\circ\mathrm{C}) = 130.00 - 29.53\Delta\delta - 23.87\Delta\delta^2 \tag{4.1}$$

For the calibration over 50°C, 100% ethylene glycol is used, whose chemical shift difference of the two peaks has a temperature dependence given by:

$$T(^\circ\mathrm{C}) = 193.0 - 101.6\Delta\delta \tag{4.2}$$

Spectrometer software may be used to calculate the temperature after the $\Delta\delta$ is measured. Since the accuracy of the measurement is greatly dependent on the line shape of the peaks, the sample should be well shimmed before the calibration. It is impossible to shim using the ^{2}H lock level by the conventional shimming method because the calibration samples do not contain any portion of deuterated solvents. Gradient shimming on ^{1}H is the best way to do the z shimmings. A sample containing about 1:1 methanol-d_4 in methanol, which has the same volume as

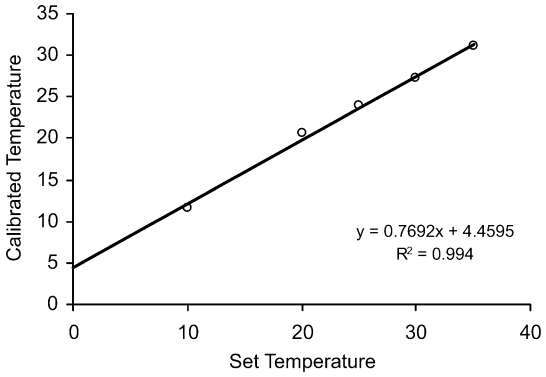

Fig. 4.3 Plot of set temperature vs. calibrated temperature (°C) using a methanol sample

the calibration sample, is first used for shimming purpose. After well shimming the methanol-d_4 sample, especially the nonspinning shims, the 100% methanol sample is placed in the probe and ^{1}H auto gradient shimming z_1–z_6 is applied. Now the sample is ready for temperature calibration. Change the temperature to the lowest point to be calibrated. It takes about 10 min for the temperature to reach equilibrium. Collect data with a single transient and calculate the temperature according to the above equation or by using the appropriate command of the instrument's software. Repeat the experiment and average the two calculated values of the calibrated temperature. Figure 4.3 shows a plot of the set temperature vs. the calibrated ones. A good VT control unit always has a linear relationship for all probes although the slope for individual probes may be different.

4.3.2 Calibration of Chemical Shift References

Tetramethylsilane (TMS) is the IUPAC standard compound used for ^{1}H and ^{13}C references for samples in organic solution (see Chap. 1). However, its insolubility in aqueous solutions makes it a poor reference sample for protein samples. For aqueous samples, DSS (2,2-dimethyl-2-silapentane-5-sulfonic acid) in 90% H_2O/10% ^2H_2O is a better standard sample for ^{1}H chemical shift reference because of its properties of high water solubility, far-upfield resonance, and insensitivity to pH and temperature. The water resonance is sometimes also used as a secondary (or indirect) ^{1}H reference. Although it is a convenient standard, the dependences of temperature and pH as well as the relatively broad line shape of water make it a controversial reference. The chemical shift of water at neutral pH is obtained by its temperature dependence in the range of 10–45°C:

$$\delta_{H_2O}(\text{ppm}) = 4.76 - (T - 25.0)0.01 \tag{4.3}$$

in which temperature T is in °C. Before the calibration is performed using any reference sample, the ^{2}H signal of ^2H_2O is adjusted to be on-resonance. The chemical shift of DDS is set to zero frequency. For heteronuclei such as ^{13}C and ^{15}N, the best method to set chemical shift reference is to indirectly reference to DSS ^{1}H frequency via the frequency ratio Ξ at 25°C (Table 1.1) rather than using universal reference standards. There is a small temperature dependence ΔΞ in the range of 5–50°C, which can be added to Ξ according the relationships:

$$\Delta\Xi^{N}(T) = (T - 25^{\circ}\mathrm{C})2.74 \times 10^{-10} \tag{4.4}$$

$$\Delta\Xi^{C}(T) = (T - 25^{\circ}\mathrm{C})1.04 \times 10^{-9} \tag{4.5}$$

As the equations indicate, the effect of temperature on the chemical shift for solution samples is extremely small. Therefore, it is generally ignored for most chemical and biological solution samples (Harris et al. 2001). If one prefers to use individual standard samples for heteronuclear chemical shift reference, the calibration can be done using DSS for ^{13}C and liquid ammonia for ^{15}N. The ^{13}C signal of DSS is directly observed and set to zero frequency. However, it is difficult to observe the ^{15}N signal of liquid ammonia because the sample is not in a liquid state at laboratory conditions of ambient temperature and pressure. Consequently, ^{15}N urea is commonly used as a secondary ^{15}N reference standard, whose chemical shift is referenced to liquid ammonia. ^{15}N urea with a concentration of 1 M in DMSO gives a ^{15}N peak at 77.6 ppm relative to liquid ammonia. Although the urea sample is in DMSO, the calibration must be done with the lock field on ^2H_2O resonance. First, the lock field is adjusted to the ^2H_2O resonance with a water sample in the probe because the real sample is in aqueous solution. Nonspinning shims should be checked before changing the sample to the urea sample. After gradient shimming with z_1–z_6 gradients, the ^{15}N spectrum is acquired without changing the lock field. It is crucial to make sure that the lock field is on resonance for ^2H_2O in order to obtain the accurate ^{15}N calibration.

The chemical shift reference is calibrated only periodically unless the magnetic field drift is substantial (which requires changing the lock frequency to correct for loss of magnetic field). How often the calibration needs to be performed depends on the stability of the instrument and magnet. Usually it is repeated twice annually if the lock frequency has not been changed.

4.3.3 Calibration of Transmitter Pulse Length

Once probe tuning and shimming have been completed, it is necessary to calibrate the pulse angle produced by a given amount of transmitter RF power, which is achieved by calibrating the 90° pulse length. The ^{1}H observe 90° pulse length should be calibrated for every sample. There are many different methods to

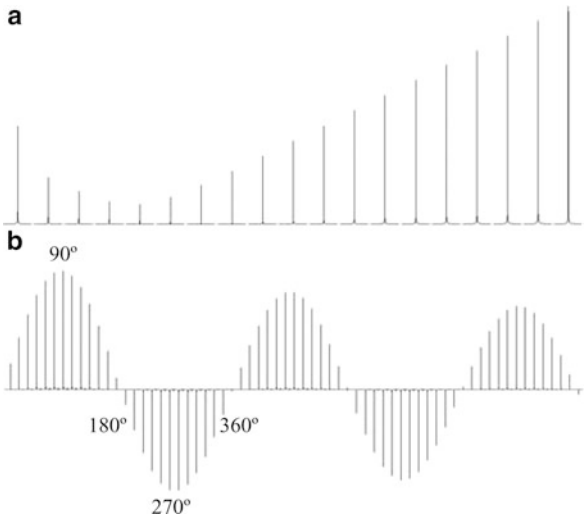

Fig. 4.4 Calibration of transmitter pulse length and offset frequency. (**a**) The offset frequency is arrayed with increment of 1 Hz using the PRESAT sequence. The minimum is obtained when the offset is on water resonance. (**b**) The pulse length is arrayed and the first minimum corresponds to a 180° pulse length

calibrate the observe pulse length. The easiest one is to calibrate a 180° pulse using a water or solvent signal. Because the maximum intensity of the observed signal by the 90° pulse is relatively insensitive to deviations of the pulse angle around 90°, the null intensity produced by a 180° pulse is commonly used to calibrate the 90° pulse length.

The calibration is performed using a one-pulse sequence with a relaxation delay longer than $5T_1$ and a single transient. The carrier frequency is set about 100 Hz from the water resonance to avoid interference of the carrier frequency with the water peak. The pulse length is arrayed by 2 μs for 15 or more FIDs to values sufficiently long to include the estimated 180° pulse length. After the first FID is transformed and phased, all FIDs are then transformed using the same phase correction. The next step is to fine array the range of pulse lengths that give signal intensity near the null value. Because of the inhomogeneity of the B_1 RF field generated at the probe coil, the signal is not completely nulled by a 180° pulse. Instead, a dispersive signal with similar amplitude of positive and negative peaks symmetric about the null position will be observed at the 180° condition (Fig. 4.4b). Sometimes a broad hump at the water resonance appears in the 180°-pulse spectrum, which is caused by the signal from the sample outside the probe coil. In the above "array" method, one is able to visualize the relationship of signal intensity with pulse length. The intensity increases with the pulse length and decreases after the pulse angle passes 90°. It passes through a null at 180° and reaches a negative maximum at 270°. This calibration can also provide information on RF field homogeneity, which is generally specified by the ratios of signal intensities at 450°/90°, and 810°/90°. However, this takes a longer time to finish.

For a quick calibration, a different method is used, which "targets" the pulse length in the range close to a previously calibrated 180° pulse. Acquire a pair of FIDs with pulse lengths of 5 μs and the estimated 180°. After Fourier transformation

of the first FID followed by phase correction, the second FID is transformed with the same phase correction. A positive intensity of the water signal in the second spectrum indicates that the pulse angle is less than 180°, whereas a negative intensity is caused by a pulse length greater than 180°. Change the pulse length accordingly to get an evenly distributed dispersive signal obtained using the same phase correction. It is good practice to check the phase correction parameters compared to the first spectrum when the calibrated 180° pulse length is unusually long or short. Similarly, a 360° pulse length can be used to calibrate the 90° pulse length by the above procedure. The 180° pulse should be checked after the 360° is calibrated, to avoid mistaking the 180° as the 360°.

An alternative way to calibrate the 90° pulse is to observe real signals of an aqueous sample rather than the water signal, using a PRESAT sequence (see solvent suppression). Because the concentration of the sample is usually very low, this method needs multiple transients, and thus takes a longer time but gives a more accurate calibration. The normal setup includes setting the saturation frequency on water resonance, number of transients to 8, steady-state transients (or dummy scans) to 4, presaturation time to 3 s and predelay of 2 s or longer, and acquisition time to 1 s. Because a full range array will take a considerably longer time, the target method is more practical to use. Once the 180° pulse length is determined, the pulse calibration is checked again with a longer predelay to ensure the accuracy of the calibration because signal accumulation with an insufficient delay can cause an incorrect measurement of intensity.

^{1}H pulses for spin locking in TOCSY and ROESY, and decoupling from ^{15}N should be applied with longer pulse length, usually approximately 25–30 μs for TOCSY, and 40 μs for ROESY and the decoupling (Table 4.1). Therefore, it is necessary to calibrate these pulses with a lower power. As discussed previously, a reduction of the power level by 6 dB results in a pulse length that is twice as long. Therefore, if the pulse length for the hard 90° pulse is approximately 7 μs, the power needs to be attenuated by 12 dB for the TOCSY spin lock pulses and by 15 dB for 40 μs pulses. The calibration can be done with any aqueous sample by arraying every 1 μs in the range near the desired pulse length.

4.3.4 Calibration of Offset Frequencies

The offset frequency (ν_{offset}) has the following relationship with the carrier frequency ν_{carr}:

$$\nu_{\text{carr}} = \nu_{\text{inst}} + \nu_{\text{offset}} \tag{4.6}$$

in which ν_{inst} is the base frequency of the instrument for the nucleus, which is the fixed frequency for a specific nucleus. For instance, ν_{inst} for ^{1}H, ^{13}C, and ^{15}N of a 600 MHz instrument is 599.5200497 MHz, 150.7747596 MHz, and 60.7557335 MHz, respectively.

Table 4.1 Common pulses used for 500 and 600 MHz instruments[a]

Pulses	On/off frequency	500 MHz		600 MHz	
		Pulse length[b]	Est. Pwr Att[c]	Pulse length[b]	Est. Pwr Att[c]
^{1}H					
^{1}H hard 90°	On	7		7	
TOCSY spin lock	On	28	12	28	12
WALTZ dec	On	40	15	40	15
^{13}C					
All ^{13}C 90° hard	On	15		15	
^{13}C GARP	On	70	14	70	14
DIPSI-3 spin lock	On	30	6	30	6
$C^{\alpha,\beta}$ 90°, C′ null	On	58.4	11–12	48.6	10
C^{α} 90°, C′ null	On	64.7	12–13	53.9	11
C′ 90°, C^{α} null	On	64.7	12–13	53.9	11
C′ 90, C^{α} null	Off	64.7	12–13	53.9	11
$C^{\alpha/\beta}$ 180°, C′ null	On	53.0	10–11	44.3	9
C^{α} 180°, C′ null	On	57.9	11–12	48.3	10
C′ 180°, C^{α} null[d]	Off	57.9 + 0.8	11–12	48.3 + 0.8	10
C^{α} 90° SEDUCE[e]	On	310.5	20	310.5	20
C^{α} 90° SEDUCE[e]	Off	310.5	20↑6	310.5	20↑6
C′ 90° SEDUCE[e]	Off	310.5	20↑6	310.5	20↑6
C′ 180° SEDUCE[f]	Off	200 + 4	16↑6	200 + 4	16↑6
^{15}N					
All ^{15}N hard 90°	On	40		40	
^{15}N GARP dec	On	250	15	250	15
^{15}N Waltz16 dec	On	200	14	200	14

[a]The pulse lengths listed in the table are used as starting values. Actual pulse lengths and powers should be calibrated accurately for the instruments

[b]The pulse lengths are calculated according to (4.14) and (4.17) using $C^{\alpha/\beta} = 45$ ppm, $C^{\alpha} = 58$ ppm, and C′ = 177 ppm, and ^{13}C frequency of 125.68 and 150.86 MHz for 500 and 600 MHz instruments, respectively.

[c]The power attenuation for the 90° pulse calibration is the decreased power in dB from the power for the hard pulse (increase the power setting value for Bruker, or decrease the power setting value for Agilent instruments). "↑6" means increase the power by 6 dB (decrease the power value by 6 for a Bruker instrument). It is estimated relative to a hard 90° of 15 μs, assuming linearity of the amplifier. The reduction of power by 1 dB increases the pulse length by a factor of 1.122

[d]After the calibration, 0.8 μs is added to the off-resonance 180° pulse length

[e]The SEDUCE 90° pulses must be divisible by 50 ns and 45°. For off-resonance SEDUCE decoupling pulses: after the calibration, the power is increased by 6 dB (decreased for a Bruker instrument) because the off-resonance SEDUCE decoupling covers a double band width

[f]After the calibration, 4 μs is added to the pulse length of the off-resonance 180° SEDUCE and the power is increased by 6 dB (decreased for a Bruker instrument)

4.3.4.1 Calibration of Transmitter Offset Frequency

Because common biological samples are in aqueous solution, the transmitter v_{offset} (e.g., o1 on a Bruker instrument and tof on an Agilent instrument) is required to be set on the water resonance for experiments with water suppression. If the transmitter v_{offset} is off by even 1 Hz, it will significantly affect the result of water suppression experiments. Therefore, v_{offset} calibration is performed for each individual sample. It is first estimated from the water peak using a one-pulse sequence by setting it on the center of water peak. It is then arrayed by 0.5 Hz in the range of ±3 Hz of the setting value using a PRESAT sequence (see solvent suppression) with 2 transients for steady state and 8 transients per FID. The correct v_{offset} gives the lowest intensity of the water peak (Fig. 4.4a). If the ^2H signal of ^2H_2O is adjusted to be on-resonance prior to ^2H locking, v_{offset} should be within the range of a few hertz for different samples at a given temperature. It may have very different values if the lock is not adjusted to be on-resonance prior to the calibration.

4.3.4.2 Calibration of Decoupler Offset Frequency

The correct decoupler offset frequency (e.g., o2, o3 on a Bruker instrument or dof, dof2 on an Agilent instrument) needs to be known before pulse calibration for the decoupler channel. A simple one-pulse experiment with continuous wave (CW) heteronuclear decoupling is used for this purpose. The power of the CW decoupling is set very low so that only a narrow frequency range (a few tens of hertz) is decoupled in order to accurately determine the value of decoupler v_{offset}. Arraying the decoupler v_{offset} in the experiment provides a series of spectra with modulated signal intensity (Fig. 4.5). As the v_{offset} becomes closer to the resonance frequency of the heteronuclear signal, the doublets become closer, resulting in an intensity increase of the peak. The maximum intensity is obtained when the v_{offset} is on or near resonance. The lower the CW power, the narrower the frequency bandwidth it decouples. The spectra shown in Fig. 4.5 were obtained with a CW RF field strength of 70 Hz. The maximum pulse power of a 300 W heteronuclear amplifier was attenuated by −42 dB, which reduced the pulse power by a factor of 128 (or 2^7).

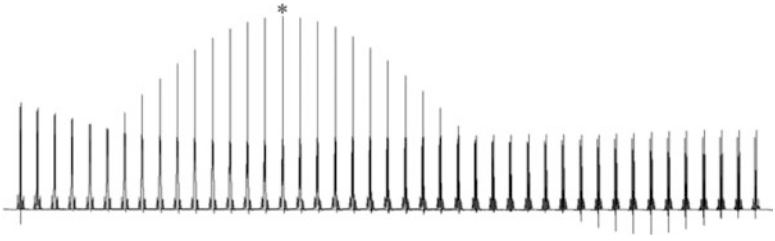

Fig. 4.5 Arrayed spectra for calibrating decoupler offset frequency using ^{15}N urea in DMSO. The decoupler offset frequency is arrayed with increments of 1 Hz as stated in the text. The spectrum labeled with an *asterisk* has the offset frequency on urea ^{15}N resonance

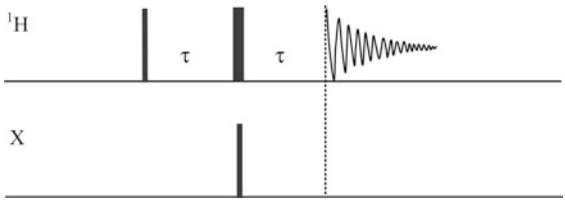

Fig. 4.6 Pulse sequence for calibrating the pulse length of the heteronuclear decoupler. The delay τ is set to $1/(2J_{HX})$. When the X pulse is 90°, the doublet has minimum intensity

(As a reminder, attenuation by −6 dB decreases RF field strength by a factor of 2.) If the bandwidth of the CW decoupling is wider than the increment of the decoupler ν_{offset} array, there will be several spectra with the same maximum intensity at the peak. The average value of the ν_{offset} in the spectra with the same maximum intensity should be taken to get the calibrated decoupler offset frequency.

4.3.5 Calibration of Decoupler Pulse Length

Decoupler pulse length is calibrated only periodically because it usually does not change from sample to sample. The calibration is performed indirectly, meaning that the effect of the decoupler pulse on the observed nuclei is calibrated. In principle, any sample enriched with ^{15}N and/or ^{13}C can be used for ^{15}N and ^{13}C decoupler pulse calibration. Samples used for the calibration include (^{15}N, ^{13}C)-NAcGly in 90% H_2O/10% ^2H_2O, 1 M ^{15}N urea in DMSO-d_6 (Dimethyl Sulfoxide-d_6), 0.1% ^{13}C methanol in 99% ^2H_2O/1% H_2O (Agilent autotest sample), or other samples for indirect calibration. The pulse sequence shown in Fig. 4.6 is one of those commonly used to calibrate ^{15}N and ^{13}C decoupler pulses. A delay τ is set to $1/(2J_{HX})$ for calibrating the decoupler pulse of heteronucleus X. J_{HX} is measured by the frequency difference between the doublets. It is important to use the correct ^{1}H 90° pulse length and the decoupler offset frequency must be set on the center frequency of the heteronuclear doublets in order to get an accurate calibration at low decoupler power.

To calibrate the decoupler pulse length, the decoupler offset frequency is set to the calibrated value which is in the center of the coupled doublets. When the angle of the heteronuclear X pulse is zero, a doublet is observed. Similar to the ^{1}H pulse calibration, the phase parameters of the first spectrum will be used for the subsequent spectra acquired by arraying the X pulse length. The 90° X pulse will give a null intensity of the doublet. The pulse length at high power is usually calibrated first, and is relatively insensitive to the deviation of decoupler offset frequency. Typical high power 90° pulse lengths for ^{13}C are approximately 15 μs, whereas those for ^{15}N can be as long as 40 μs. When calibrating the high power X pulses, although the maximum allowed B_1 RF field strength (pulse power) can be used, a pulse power that is 3 dB less than the maximum RF power is commonly chosen because it is in the linear range of the amplifier. However, a properly chosen pulse power is the one that gives the above short pulse length.

The 90° pulses for heteronuclear decoupling use much less power and, hence, have a longer pulse length. For example, the desired ^{13}C 90° pulse for GARP

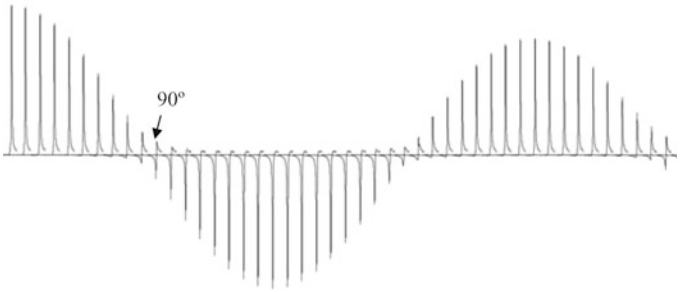

Fig. 4.7 Arrayed spectra for decoupler 90° pulse calibration. The 90° pulse gives minimal intensity

decoupling is 70 and 300 μs for SEDUCE decoupling, and ^{15}N 90° decoupling pulses are 200–250 μs for WALTZ-16 or GARP. Therefore, the decoupling pulses are calibrated with a lower decoupler power. The linearity of the amplifier can be used to estimate the power for the desired pulse length, based on the relationship given by:

$$\mathrm{dB} = 20 \log_{10}(\mathrm{pw}_1/\mathrm{pw}_2) \tag{4.7}$$

in which pw_1 and pw_2 are the pulse lengths for the hard 90° pulse and the 90° decoupling pulse, respectively. If pulse power is decreased by 1 dB, the pulse length is increased by a factor of 1.122 linearly:

$$1\ \mathrm{dB} = 10^{1/20} \approx 1.122 \tag{4.8}$$

Therefore, N dB reduction in pulse power lengthens the pulse by a factor of $(1.122)^N$. This equation is equivalent to (2.2) in Chap. 2 (on Instrumentation) because the pulse length is proportional to the B_1 field strength, or the voltage. Specification test data and previous calibration are also reasonable references to estimate the decoupler power setting. For the calibration of low power decoupling pulses, the pulse length is set to the desired value, for example, 70 μs for ^{13}C or 250 μs for ^{15}N (Table 4.1). Then the decoupler power is arrayed by 1 dB from lower power to higher in a range of 10 dB (lower power means a smaller value of the power setting for an Agilent spectrometer and a larger value for a Bruker spectrometer). When the power is lower, the selected pulse length is less than that of a 90° pulse, resulting in a doublet with positive phase. Phase the first spectrum obtained at the lowest power so that it has a doublet with correct phase. Then all FIDs are transformed using the same phase parameters as the first one. The intensity of the doublet will decrease as the power increases. The power corresponding to the intensity closest to null is used to calibrate the pulse length. The next step is to array the pulse length with the calibrated power in the range of 70 ± 10 μs by a step of 1 μs for ^{13}C, or 250 ± 50 μs by a step of 4 μs for ^{15}N, to get the 90° pulse length at the calibrated power. When calibrating the pulses, the relaxation delay must be sufficiently long and the decoupler ν_{offset} must be calibrated to be in the center of the doublet. Figure 4.7 shows the spectra obtained with correct delay and decoupler ν_{offset}.

4.3.6 Calibration of Decoupler Pulse Length with Off-Resonance Null

In certain triple resonance experiments, it is desirable to excite one region of ^{13}C resonances but not others. The range of resonances is usually centered at 58 ppm for C^{α}, 177 ppm for carbonyl carbon C′, and 45 ppm for $C^{\alpha/\beta}$. In HNCO experiment (see the following chapter), for example, the carrier of the ^{13}C is set on C′. A 90° pulse on C′ with null at C^{α} has a pulse length given by:

$$\tau_{90,\text{null}}(\ \mu\text{s}) = \frac{0.96825}{\Omega} \times 10^6 \tag{4.9}$$

in which Ω is the frequency difference in Hz between the center of C′ and C^{α}:

$$\Omega = \nu_{C'} - \nu_{C^{\alpha}} = (\delta_{C'} - \delta_{C^{\alpha}})\nu_{\text{ref}} \tag{4.10}$$

in which $\nu_{C'}$ and $\nu_{C^{\alpha}}$ are the center frequencies of C′ and C^{α} in Hz, respectively, $\delta_{C'}$ and $\delta_{C^{\alpha}}$ are the spectral centers in ppm, and ν_{ref} is the reference frequency of the ^{13}C chemical shifts in MHz. Assuming that a 600 MHz spectrometer has a ν_{ref} of 150.86 MHz for ^{13}C, $\Omega = (177 - 58)*150.86 \approx 17{,}950$ Hz, which gives a pulse length of 53.9 μs.

The effect of a hard 90° pulse on the spins is different when on-resonance and off-resonance. If on-resonance, the 90° pulse length is solely produced by B_1 field because nuclear spins experience only the B_1 field:

$$\gamma B_1 \text{pw} = \frac{\pi}{2} \tag{4.11}$$

in which pw is the pulse length, $\gamma B_1 = \omega_1$ which is the frequency of B_1 field. As the resonance frequency moves away from the carrier, the effective field is the vector sum of B_1 and the field along the z direction with the field strength $2\pi\Omega/\gamma$ as a function of the frequency difference Ω and nuclear gyromagnetic ratio γ:

$$\gamma B_{\text{eff}} = \sqrt{(\gamma B_1)^2 + \left(\gamma \frac{2\pi\Omega}{\gamma}\right)^2} \tag{4.12}$$

The simplest way for an on-resonance 90° pulse to be a null pulse at Ω Hz off-resonance is to generate a 360° (or 2π) pulse at the off-resonance frequency. Under this condition, pw must satisfy the following relationship in the same way as the on-resonance pulse does:

$$\sqrt{(\gamma B_1)^2 + (2\pi\Omega)^2}\,\text{pw}_{90} = 2\pi \tag{4.13}$$

in which $\gamma B_1 = \pi/(2\ \mathrm{pw}_{90})$ according to (4.11) and pw_{90} is the on-resonance 90° pulse length. By substituting γB_1 with $\pi/(2\ \mathrm{pw}_{90})$ and rearranging the equation, the pulse length that gives 90° on-resonance and null (360°) off-resonance has a value determined by:

$$\mathrm{pw}_{90} = \frac{\sqrt{15}}{4\Omega} \tag{4.14}$$

For the case that the frequency difference Ω between C' and C^{α} is 17,950 Hz, pw_{90} is 53.9 μs.

Similarly, a 180° pulse is generated by the B_1 field on resonance:

$$\gamma B_1 \mathrm{pw}_{180} = \pi \tag{4.15}$$

When the 180° pulse is needed to give a 360° pulse angle at Ω Hz off-resonance it must satisfy the following condition:

$$\sqrt{\left(\frac{\pi}{\mathrm{pw}_{180}}\right)^2 + (2\pi\Omega)^2 \mathrm{pw}_{180}} = 2\pi \tag{4.16}$$

After the equation is rearranged, the pw_{180} can be determined by:

$$\mathrm{pw}_{180} = \frac{\sqrt{3}}{2\Omega} \tag{4.17}$$

With a Ω of 17,950 Hz, pw_{180} is 48.3 μs. In practice, if pw_{180} is used for off-resonance excitation, it is set to be 0.8 μs longer than the calibrated value, which is 49.1 μs.

The 90° and 180° hard pulses mentioned above are used to rotate the magnetization at the frequencies on resonance and do not change the magnetization (360° rotation) at the off-resonance region Ω Hz away from the carrier frequency. In the cases when perturbation of the off-resonance frequencies is desired, which generates 90° or 180° rotation of the magnetization at off-resonance frequencies without exciting the region at the carrier frequency, shaped hard pulses are used, which are generated using the calibrated pw_{90} or pw_{180} (see Sect. 4.4). The desired pulse lengths for decoupler off-resonance pulses are calibrated by arraying the pulse power using the pulse sequence for decoupler pulse calibration. In most cases, it is necessary to calibrate fine attenuation of the decoupler power in order to obtain the desired pulse length.

4.4 Selective Excitation with Narrow Band and Off-Resonance Shaped Pulses

In many experiments, a certain frequency region must be excited without disturbing the magnetization at other frequencies. Selective pulses that have a narrow excitation range are utilized to selectively excite a group of nuclei, such as protons of

water molecules or a kind of carbons of proteins. They are referred to as soft pulses as opposed to hard pulses that have a wide excitation range and cover all the nuclei of the same isotope, such as ^{1}H, ^{13}C and ^{15}N. Applications of selective pulses include improving solvent suppression, reducing spectral width so as to increase digital resolution in multidimensional experiments, and selectively exciting frequency regions of different spins such as C' and C^{α}. A nonselective pulse, or hard pulse, is generated by a high power for a short time. The shorter the hard pulse, the wider the excited frequency range (see Sect. 1.5.1). As an approximation, the bandwidth of a pulse can be considered as the frequency range of its Fourier transformation, and it is inversely proportional to the pulse length. The Fourier transformation of an infinitely long time function gives a delta function in frequency domain. Therefore, a narrow excitation bandwidth can be achieved by reducing the pulse power and increasing pulse length. Such a selective pulse is utilized in solvent suppression by presaturation to saturate the transition of water spins. However, a desirable selective pulse should have properties such as a relatively short pulse length, a narrow excitation region covering the desired frequencies, a uniform excitation band, and linear phase dependence of transverse magnetization on the frequency offset. Amplitude-modulated and/or phase-modulated pulses, called shaped pulses, are used to generate selective pulses with the desired characteristics.

Although the pulse shape cannot be directly determined from the desired excitation profile due to the nonlinearity of the NMR response governed by the Bloch equations, Fourier transformation is a convenient method to design the pulse shape based on the desired excitation profile (Emsley 1994). The Gaussian function has a unique characteristic that the Fourier transformation of a Gaussian is also a Gaussian. It is for this reason that the Gaussian has been used as a shaped pulse for selective excitation (Bauer et al. 1984). Another example is a sinc (sine x/x) function that has a semirectangular frequency response, which is another application of the Fourier similarity theorem. A 90° Gaussian shaped pulse can be used to rotate the magnetization by 90° within the excitation bandwidth of the shaped pulse. However, the rotated off-resonance magnetization gradually dephases during the pulse, which produces a significant phase difference between the on-resonance and off-resonance magnetization (within the excitation bandwidth). When a Gaussian 90° pulse is used for selective excitation of solvent magnetization, this phase error does not cause any problem because the bandwidth of the pulse is narrow and the solvent magnetization is not desired to be observed. The problem arises if the Gaussian 90° is used to selectively excite a region of particular spin magnetization (e.g., C' or C^{α}).

A simple solution to the phase error is to use a 270° Gaussian pulse that rotates the magnetization by 270° rather than 90° (Emsley and Bodenhausen 1989). The 270° pulse improves the phase response significantly compared to the 90° pulse. The improvement can be understood as the following. When applying a 90° Gaussian pulse on y axis, the on-resonance magnetization is rotated onto the x axis, whereas the magnetization at an offset from the resonance lands near the y axis, resulting in a nearly 90° phase difference between the magnetizations of on- and

off-resonance. On the other hand, if the on-resonance magnetization is rotated by a 270° Gaussian pulse to pass the x axis, the $-z$ axis, and reach on $-x$ axis, the off-resonance magnetization is, through a different route, rotated to a position very close to $-x$ axis. The net result is that both the on- and off-resonance magnetizations are rotated to the $-x$ axis and phase error is reduced. Thus, a 270° Gaussian pulse produces an approximate in-phase excitation, which is sufficient for common applications in NMR spectroscopy of biological macromolecules. Other popular selective shaped pulses that provide improved in-phase excitations include half Gaussian (Friedrich et al. 1987; Xu et al. 1992), e-BURP-2 (Geen and Freeman 1991), and G^4 Cascade (a sum of Gaussians, Emsley and Bodenhausen 1990). The functions require a number of variable parameters to be defined, as many as 12 or more. The parameters can be optimized by software using pulse power and pulse length to produce the desired shaped pulse with desired excitation bandwidth and offset.

In order for NMR spectrometer hardware to utilize the shaped pulse function, the shaped pulse consists of a series of short rectangular pulses (a few microseconds) with different amplitudes. The duration of the shaped pulse is the sum of the pulse lengths of the element pulses. The shape is approximated by the amplitudes of the element pulses. A typical text file of a shaped pulse profile lists sequentially the individual width and power for each element pulse.

Like other pulses, the shaped pulse must be calibrated every time the sample is placed in the magnet if it is a transmitter pulse or periodically if it is a decoupler pulse. If the pulse length changes, the shaped pulse needs to be regenerated using the correct pulse length. This means that the transmitter shaped pulse will be regenerated more frequently than we prefer. One way to avoid the regeneration of the shaped pulse is to calibrate the pulse power for the fixed pulse length used by the shape function so that the existing shaped pulse function can be used. If the pulse length used in the existing shaped pulse is known, the conventional method is to calibrate the pulse power for the desired duration of the rectangular pulse. If the pulse length used to generate the shaped pulse is unknown, the shaped pulse itself must be used for the calibration.

For the calibration of the shaped pulse, the pulse length and pulse power used to generate the shaped pulse profile would be good reference values. For a 180° shaped pulse, the calibration can be performed using a one-pulse sequence in which the shaped pulse is defined as the same shape pulse profile to be used in the experiment. The correct pulse power for the desired pulse length is determined by arraying the fine power attenuation, which gives a dispersive residual signal. In general, a 90° shaped pulse cannot be obtained by dividing the calibrated 180° shaped pulse length or by doubling the power. A pulse sequence containing one hard 90° pulse and one shaped pulse (or two identical 90° shaped pulses) with the same phase is used for the 90° shaped pulse calibration. The sequence achieves 180° rotation of the magnetization around the axis. Arraying the pulse power using the same procedure in the 180° pulse calibration is performed to determine the power for the 90° shaped pulse.

4.5 Composite Pulses

RF pulses are used to rotate magnetization at desired angle, frequency, and duration. For certain applications, pulses are combined together to form a pulse train with or without delay in between pulses to accomplish specific functions. The pulse trains are called composite pulses. The applications of composite pulses range from improving imperfections of single pulses, spin lock for magnetization transfer to off-resonance excitation, and spin decoupling.

4.5.1 Composite Excitation Pulses

To compensate for the effects of off-resonance and RF field inhomogeneity, and to produce effective magnetization rotation by a specified angle, numerous composite pulses have been developed. Among them, the composite pulses for 90° and 180° excitation are more frequently utilized in biological NMR spectroscopy. The most commonly used composite pulses consist of a few 90° and/or 180° pulses varying in phase. The pulse sequence $90_x90_y90_{-x}90_{-y}$ is a popular version of a composite 90° pulse used as a read out pulse (last pulse in the sequence) in certain NMR experiments with solvent suppression. The composite 180° pulse containing a sequence of $90_x180_y90_x$ is sometimes used to improve the performance in inversion of z magnetization in a pulse sequence.

4.5.2 Composite Pulses for Isotropic Mixing

The Hartmann–Hahn matching condition (Hartmann and Hahn 1962) is required to be satisfied during the coherence transfer between spins by isotopic mixing in TOCSY experiments (see TOCSY for detail). When the scalar coupled spins have different frequency offset from the B_1 carrier frequency, the efficiency of the magnetization transfer produced by the continuous RF field is extremely low. The required power of the RF field to cover a frequency range to satisfy the Hartmann–Hahn matching condition would produce a tremendous amount of heat during the period of mixing, which would overheat the probe and damage the NMR samples. Several pulse sequences for Hartmann–Hahn mixing have been developed to achieve effective coherence transfer. MLEV17 (Bax and Davis 1985a, b) and WALTZ16 (Shaka et al. 1983a, b) are the early versions, which utilize phase-modulated pulses. WALTZ16 combines basic elements of the sequences into supercycles to improve the transfer efficiency. Later, delays were added into the MLEV17 sequence in clean-TOCSY experiments to improve the performance (Griesinger et al. 1998). It has been found that the clean-TOCSY mixing scheme

produces more heat during the mixing period and can cause overheating problem, which is not suitable for experiments with a long mixing time.

The mixing sequences commonly used in multidimensional NMR spectroscopy are DIPSI sequences that consist of pulses with different pulse angles (Shaka et al. 1988; Rucker and Shaka 1989). The DIPSI-2 and DIPSI-3 sequences provide much better efficiency of coherence transfer than phase-modulated sequences, MLEV17 and WALTZ16. For all of the composite pulse sequences, only the 90° pulse length needs to be calibrated. The sequences take the 90° pulse length and convert it into other pulse angles if necessary. A pulse length of the 90° pulse in the range of 25–30 μs is sufficient for the majority of applications to homonuclear magnetization transfer in multidimensional NMR spectroscopy.

4.5.3 *Composite Pulses for Spin Decoupling*

Nuclear scalar coupling can be removed by applying continuous RF irradiation. This technique is commonly used in a 1D ^{1}H homonuclear decoupling experiment. However, because of the off-resonance effect, it requires very high power to obtain effective decoupling over the broadband of heteronuclear frequencies using a continuous RF field. The decoupling efficiency of a continuous RF field is described in term of the scaling factor λ as:

$$\lambda = \frac{2\pi\Omega}{\sqrt{(\gamma B_1)^2 + (2\pi\Omega)^2}} \tag{4.18}$$

in which Ω is the offset frequency in Hz from the carrier frequency, γB_1 is the frequency of B_1 field. The value of $\lambda = 0$ represents complete decoupling, whereas $\lambda = 1$ provides no decoupling effect. In order to obtain complete decoupling using a continuous wave RF field, the field must be set on resonance, that is, $\Omega = 0$. The decoupling power of CW would be required to be higher to decouple a frequency range which is offset Ω from the carrier. Only a small portion of the scalar coupling is decoupled when the offset is about the same amplitude as the applied field ($\lambda = 0.707$ when $2\pi\Omega = \gamma B_1$).

One of the major applications of composite pulses is to perform spin decoupling. The spin decoupling is achieved by the inversion of spin magnetization, based on the assumption of instant flip approximation that the spin magnetization being decoupled is inverted instantly when the frequency of the RF pulse matches its Larmor frequency. To minimize the RF power and increase the decoupling bandwidth, composite pulse sequences including some of the sequences used for isotropic mixing are utilized for heteronuclear decoupling, of which WALTZ16, GARP (Shaka et al. 1985), SEDUCE (Coy and Mueller 1993) and DIPSI-3 are popular decoupling sequences. All of them use supercycles to improve the

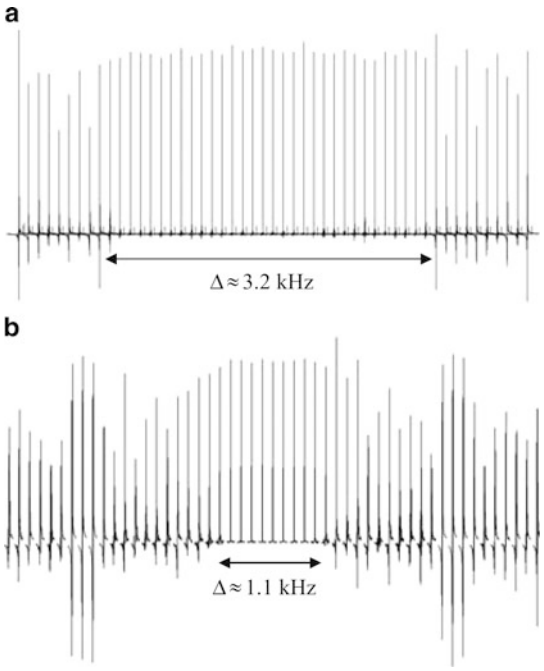

Fig. 4.8 Bandwidth of (**a**) GARP and (**b**) WALTZ16 decoupling. The $^{1}H–^{15}N$ doublets of ^{15}N urea in DMSO were observed using 51 decoupler offset frequencies with an increment of 100 Hz. (**a**) The decoupler 90° pulse length of 198 μs used in the experiments, which gives a B_1 field strength of 1.26 kHz. (**b**) 275 μs was used for the decoupler 90° pulse length, which corresponds to a B_1 field strength of 0.9 kHz. The observed decoupling bandwidths are indicated below the spectra (obtained using (4.19)). WALTZ16 has a decoupling efficiency of 1.2, whereas the observed bandwidth of GARP indicates a decoupling efficiency of 2.5

decoupling efficiency. Often the decoupling efficiency of the sequences is described by the factor of the decoupling bandwidth Δ (in units of Hz) to the strength of the applied field:

$$f_{\mathrm{d}} = \frac{2\pi\Delta}{\gamma B_1} = \frac{\Delta}{1/(4\mathrm{pw}_{90})} \tag{4.19}$$

in which pw_{90} is the 90° pulse length at the field strength $1/(4\ \mathrm{pw}_{90})$ (in Hz) and f_{d} is the decoupling efficiency. It has theoretically been demonstrated that GARP produces the decoupling bandwidth by a factor of 2.5 over the field power it uses, whereas WALTZ16 gives the same bandwidth as the field power used. The decoupling profiles of the sequences observed experimentally are shown in Fig. 4.8. In multidimensional NMR spectroscopy, GARP is usually used for ^{13}C or ^{15}N broadband decoupling, SEDUCE for selective decoupling such as C^{α} decoupling during the experiment, and WALTZ16 is used for ^{15}N decoupling.

4.6 Adiabatic Pulses

The above composite pulses are regarded as linearly polarized waveforms which are phase-modulated RF pulses. There is another type of RF pulses whose waveforms are described as circularly polarized, referred to as adiabatic pulses. They are much more efficient for inversion of spin magnetization than the phase-modulated pulses. The advantages of adiabatic pulses are their wider band width with a minimum power and their insensitivity to inhomogeneity of B_1 field. The basic idea behind them is that if the change in the orientation of the effective field with time is sufficiently slow, the tilt angle θ of the magnetization with respect to the moving direction of the effective field is very small, with the duration of the pulses shorter than any relaxation process of the system (Abragam 1961; Kupče 2001):

$$\frac{1}{T_2^*} \ll \frac{\partial \theta}{\partial t} \ll \omega_{\text{eff}} \tag{4.20}$$

This means that the change in direction of the B_1 field must be sufficiently slower than the rotation of magnetization around the effective field. Initially, the B_1 field is turned on with a frequency far away from the resonance; the effective field B_{eff} is virtually parallel to the B_0 and the magnetization is along the effective field. The frequency of the B_1 field is then changed to approach the resonance at a rate sufficiently slow so that the magnetization changes its direction to follow the direction of B_{eff} (Fig. 4.9).

A dimensionless factor Q, called the adiabaticity factor, has been introduced to quantitatively describe the adiabatic condition (Baum et al. 1985):

$$Q = \frac{\omega_{\text{eff}}}{\dot{\theta}} \tag{4.21}$$

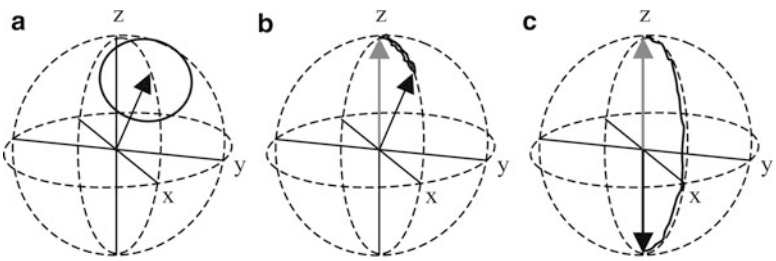

Fig. 4.9 Magnetization trajectories when RF pulses are applied (from Kupče 2001). (**a**) When the RF pulse is applied suddenly, the magnetization is rotated around the B_{eff} (*arrow*). (**b**) When the RF field is turned on adiabatically, the magnetization follows the B_{eff}, stays locked along the B_{eff} for most of time and then is returned back to equilibrium. (**c**) When the RF field is swept through the resonance frequency adiabatically, the magnetization follows the B_{eff} to the $-z$ axis and becomes inverted (reproduced with permission from Kupče 2001, Copyright © 2001 Elsevier)

in which $\dot{\theta} = \partial\theta/\partial t$. Equation (4.21) can be rewritten in terms of pulse field strength ω_1 and frequency offset Ω:

$$Q = \frac{\left(\omega_1^2 + \Omega^2\right)^{3/2}}{\omega_1\dot{\Omega} + \dot{\omega}_1\Omega} \tag{4.22}$$

in which the dot represents the rate of changing. Therefore, the adiabatic condition requires $Q \gg 1$, meaning that ω_{eff} is much greater than θ in (4.21).

Numerous adiabatic pulses whose amplitudes, phases, or both can be modulated have been developed for applications to spin decoupling, magnetization inversion, refocusing, and selective excitation. For instance, WURST (wideband uniform rate and smooth truncation, Kupče and Freeman 1995a) is an adiabatic pulse generated by adiabatically modulating the amplitude waveform of the B_1 field with the frequency offset swept linearly, according to the relationship:

$$B_1(t) = B_1^{\max}[1 - |\sin(\beta t)|^n] \quad -\frac{\pi}{2} < \beta t < \frac{\pi}{2} \tag{4.23}$$

The higher the value of n, the higher the bandwidth. WURST-20 has an n value of 20, and has been used for the inversion of magnetization to yield a uniform profile over a wide frequency range. On the other hand, both the amplitude and frequency sweep can be modulated in a coherent fashion, such as in hyperbolic secant (or sech) pulses (Kupče and Freeman 1995b; Tannus and Garwood 1996). The amplitude waveform and frequency sweep of B_1 are modulated in a hyperbolic secant pulse with the forms of:

$$\begin{aligned} B_1(t) &= B_1^{\max}\ \text{sech}(\beta t) \quad -\frac{\pi}{2} < \beta t < \frac{\pi}{2} \\ \Delta\omega(t) &= -\mu\beta\ \tanh(\beta t) \end{aligned} \tag{4.24}$$

The excitation profile and bandwidth ($\Delta\omega_{\text{BW}} = 2\mu\beta$) of the pulse is determined by the parameter μ in combination with β. As the value of μ increases, both the shape and bandwidth of the excitation are improved significantly (Fig. 4.10). The advantage of the adiabatic pulse for spin inversion is that the inversion is insensitive to the B_1 field strength and can have much more tolerance to the missetting of the B_1 field strength. Consequently, it is not affected by the inhomogeneity of either the B_1 or the B_0 fields during the experiment. Therefore, adiabatic pulses have found many applications in heteronuclear experiments in which inversion of the heteronuclear magnetization is needed such as HSQC and HMQC (see Chap. 5). They have become more and more popular in biological NMR spectroscopy.

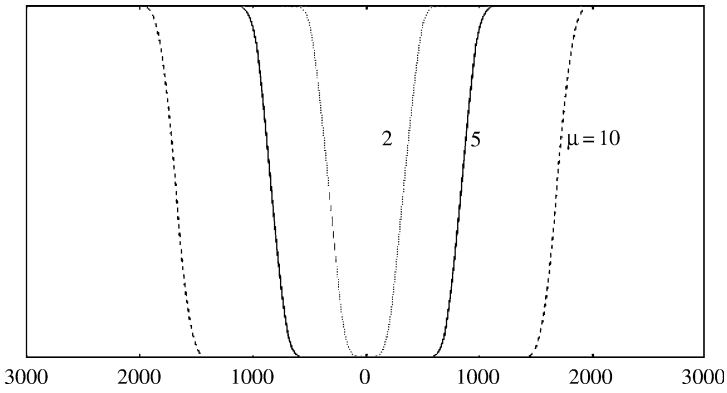

Fig. 4.10 Inversion profiles of hyperbolic secant pulses with different value of parameter μ as indicated. Higher μ generates wider bandwidth and flatter profile (reproduced with permission from Norris 2002, Copyright © 2002 Wiley Publishers)

4.7 Pulsed Field Gradients

In NMR experiments RF pulses are utilized to rotate the magnetization and create coherence transfers. Different coherence transfer pathways can be produced in the same pulse sequence. In order to extract a specific type of information, certain pathways must be separated from others. Phase cycling is a method used to select the desired coherence transfer pathway, in which the phases of pulses are systematically altered from one FID to another so that the unwanted pathway will be removed at the end of phase cycling during data acquisition. The method can be incorporated in a majority of experiments and provides satisfactory results (see Sect. 4.10.3). However, in this method, all types of magnetization (wanted and unwanted) must be collected first and then the unwanted coherence is removed via the differentiation of the data. In order to achieve this, the instrument is required to be perfect in stability and dynamic range.

PFGs have been chosen as an alternative method to select a desired coherence transfer pathway in NMR experiments. They provides several advantages over the phase cycling method in that only the desired magnetization is observed during data acquisition in each experiment, resulting in an increase in acquisition dynamic range, reducing artifacts caused by instrument instability, and shortening experimental time. Gradients also provide new methods for solvent suppression, sensitivity enhancement, and diffusion study.

When a gradient varying linearly, for example on the z axis, is applied, it causes spatial inhomogeneity of the magnetic field along the axis. The spins in different z locations experience different magnetic field strengths, which causes the spin to precess at different frequencies for chemically equivalent spins. This means that the transverse magnetization of the spins will have different precession frequencies for

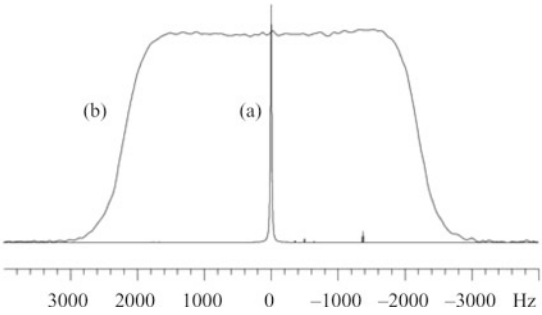

Fig. 4.11 ^{1}H spectra of water (a) without and (b) with gradients during acquisition. The intensities of the two spectra are not proportional. When the gradient is turned on, water across the sample experiences different magnetic field strengths due to the linear z gradient. Therefore, the chemical shifts are different as a function of the z position of the sample (see (4.30)). The center of the sample has zero frequency shift

different physical locations along the z axis in the sample volume. Some will precess faster, and some slower than the resonance frequency. The transverse magnetization of the spins across the sample volume will be decreased with the duration of the gradient irradiation, because a certain portion of the magnetization will be canceled out due to dephasing of the magnetization. At some time during the gradient irradiation, the transverse magnetization becomes zero. Therefore, the field inhomogeneity created by a gradient (z gradient) eliminates the magnetization on the plane (xy plane) perpendicular to the gradient axis. The process may be reversed to recover the dephased magnetization by applying the gradient with an opposite direction, or negative to the previous gradient with the same duration. When the gradient reverses the direction of the gradient field, the spins precessing slower under the previous gradient field will now precess faster, whereas those that were slower will now precess faster. After the same duration that caused the magnetization to disappear, the magnetization will regain its original amplitude, if ignoring relaxation effects. The former process is called dephasing, while the latter is called refocusing.

If the z gradient in a one-pulse experiment is applied during acquisition of signal from a single resonance, the observed FID is a sinc-type function. The pulse sequence is utilized by gradient shimming method. After Fourier transformation, a spectrum with a flat step shape is obtained (Fig. 4.11). The frequency range is symmetric about the resonance frequency in the absence of the gradient (the center of the spectrum) because the origin of the gradient field is in the center of the probe coil. The magnetic field, B_g, across the sample created by a gradient pulse on the z axis is a linear function of the position along the z direction (Keeler et al. 1994):

$$B_g = zG \tag{4.25}$$

in which G is the gradient field strength in units of Gauss per centimeter, Gcm^{-1}, or tesla per meter, Tm^{-1}. The convenient and commonly used unit is Gcm^{-1} because

gradient coils in NMR probes are a few centimeters in length. During the experiments, the field strength of the gradients is defined in terms of digital units such as DAC (digital-to-analog conversion). In order to set the gradient to specific strength in units of Gcm^{-1}, the maximum gradient strength corresponding to the maximum DAC unit must be known. For instance, if the maximum gradient strength of a probe is 70 Gcm^{-1} and the setting range of the gradient is from 32k DAC to −32k DAC, 8,000 DAC represent a gradient strength of 17 Gcm^{-1}. The field strength at a given position z of the sample is described by:

$$B = B_0 + B_\mathrm{g} \tag{4.26}$$

Because B_0 will contribute evenly over the sample, we will drop the term and only consider in the rotating frame the effect of the gradient on the sample at different positions. The precession frequency of spins at any specific sample position z under the interaction of the gradient field is given by:

$$\omega_\mathrm{g} = \gamma B_\mathrm{g} = \gamma z G \tag{4.27}$$

in which ω_g is the precession frequency of the spins in the presence of B_g. The phase of the precession at the sample position z after the gradient field G is applied for a period of time t is determined by:

$$\phi(z) = \gamma z G t \tag{4.28}$$

Considering the above example in which a single peak is present in the spectrum, x magnetization of spins at any specific sample position z evolves after applying a z gradient for time t:

$$M_x(z) \xrightarrow{\gamma z G t} \cos(\gamma z G t) M_x(z) + \sin(\gamma z G t) M_y(z) \tag{4.29}$$

$M_x(z)$ is the transverse x magnetization at sample position z, which is dependent on the gradient strength and pulse time t. The appearing x magnetization comes from all of the sample slices along the z direction, and is the average over all sample slices. Because the origin of the gradient field is at the center of the sample, the integration (summation) of the $M_x(z)$ is from $-½r_\mathrm{max}$ to $½r_\mathrm{max}$ for a length of r_max (Fig. 4.12):

$$\begin{aligned} M_x &= \frac{1}{r_\mathrm{max}} \int_{-\frac{1}{2}r_\mathrm{max}}^{\frac{1}{2}r_\mathrm{max}} \cos(\gamma z G t)\, \mathrm{d}z = \frac{2\sin\left(\frac{1}{2} r_\mathrm{max} \gamma G t\right)}{r_\mathrm{max} \gamma G t} \\ &= \mathrm{sinc}\left(\frac{1}{2} r_\mathrm{max} \gamma G t\right) \end{aligned} \tag{4.30}$$

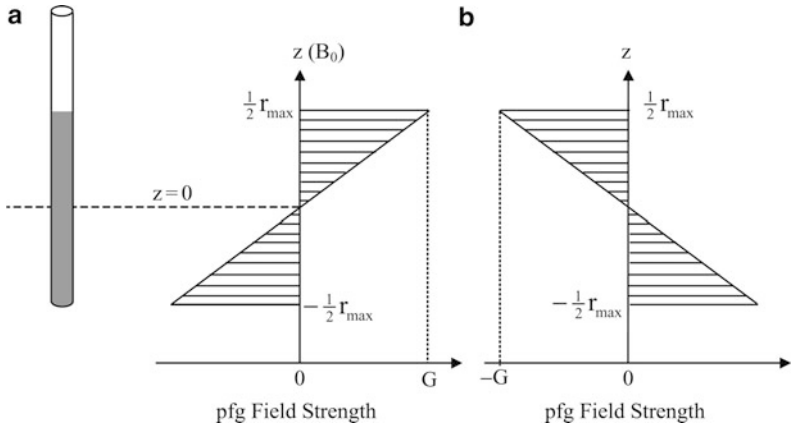

Fig. 4.12 The z gradient field strength across the sample volume. The origin of the gradient field is in the center of the sample (precisely, it is in the center of probe coil). The gradient field strength is a linear dependence of the z positions of the sample volume, and the total length along z axis is r_{max}. (**a**) The field strength distribution when a G gradient is applied. (**b**) The gradient field strength when a $-G$ gradient is applied. The sign of the gradients is relative

If the gradient pulse is applied during the entire acquisition time, the observed FID is a sinc function as described in (4.30). Fourier transformation of the sinc FID gives a spectrum with a broad range of frequencies caused by the gradient (spectrum b in Fig. 4.11). The width of the frequency band depends on the strength of the gradient. Because the origin of the gradient is at the center of the sample, the frequency distribution is symmetric about the resonance frequency as shown in the spectrum.

In multipulse experiments, a 180° pulse is frequently used to invert z magnetization $M_z \rightarrow -M_z$ (for instance, 180° decoupling pulse) or to generate a spin echo, that is, change the sign of the coherence order, $p \rightarrow -p$ (see Sect. 4.10.3). An imperfect 180° refocusing pulse is a noticeable source of pulse artifacts that can be removed by the phase cycling method EXORCYCLE (Bodenhausen et al. 1977). Gradient pulses can also be used to eliminate artifacts from an imperfect 180° refocus pulses. For a 180° inversion pulse, the first gradient pulse is applied before the 180° pulse to dephase the transverse magnetization (Fig. 4.13a), whereas the longitudinal magnetization is not influenced by z gradient pulses. After the 180° the second gradient pulse with opposite sign is applied to dephase any transverse magnetization produced by an imperfect 180° excitation. The opposite sign is used to avoid refocusing the transverse magnetization dephased by the first gradient pulse so that it is continuously dephased during the second gradient.

To remove artifacts during the inversion of coherence order by an imperfect 180 refocusing pulse, the coherence of order p is selected by a pair of gradient pulses (Fig. 4.13b). The 180° pulse inverts the order of the coherence after the first

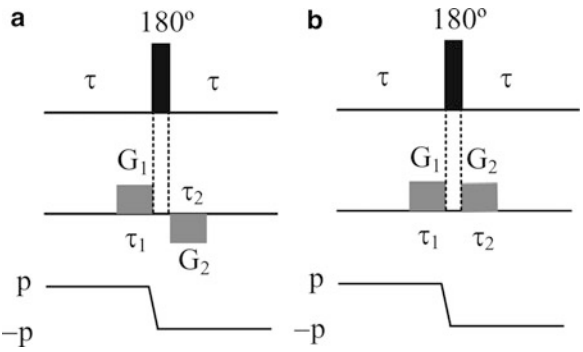

Fig. 4.13 Elimination via gradient pulses of artifacts due to imperfect 180° pulses. (**a**) Gradient-enhanced spin inversion sequence in which the artifacts are removed by a pair of *z* gradient pulses with opposite sign. The gradient pulses sufficiently dephase transverse magnetization while the longitudinal magnetization is not disturbed by the *z* gradient pulses. The opposite sign of the second gradient pulse is used to avoid refocusing any transverse magnetization dephased by the first one. (**b**) Gradient-enhanced spin echo sequence using gradient pulses to select the coherence echo so that the artifacts from the imperfect 180° pulse are removed. The gradient pulses are applied with the same strength and duration ($G_1\tau_1 = G_2\tau_2$) to accomplish the selection of the coherence with order of $-p$. Any coherence of order other than -1 generated by the 180° pulse is removed after the second gradient pulse

gradient pulse dephases the coherence. The second gradient pulse is applied to refocus the coherence according to the coherence selection rule:

$$G_1\tau_1 p + G_2\tau_2(-p) = 0 \tag{4.31}$$

$$G_1\tau_1 = G_2\tau_2 \tag{4.32}$$

The second gradient pulse is applied with the same strength, duration and sign as the first one. Any coherence with order other than $-p$ will sufficiently be removed during the second gradient pulse. For both methods, the artifacts are effectively eliminated by a single transient without any phase cycling. The reduction of phase cycling translates to faster data acquisition or higher digital resolution through the collection of more increments in the indirect dimensions. The selection of coherence transfer pathways by gradients is discussed in more detail in Sect. 4.10.3.

4.8 Solvent Suppression

In order to observe amide protons which contain rich structure information, it is necessary to dissolve protein samples in aqueous buffer solution containing only approximately 5% ^2H_2O for ^2H lock. It is difficult to observe the signals from the solute in the presence of the intense signal from water protons since water protons in 95% aqueous solution with a concentration of approximately 105 M have bulk

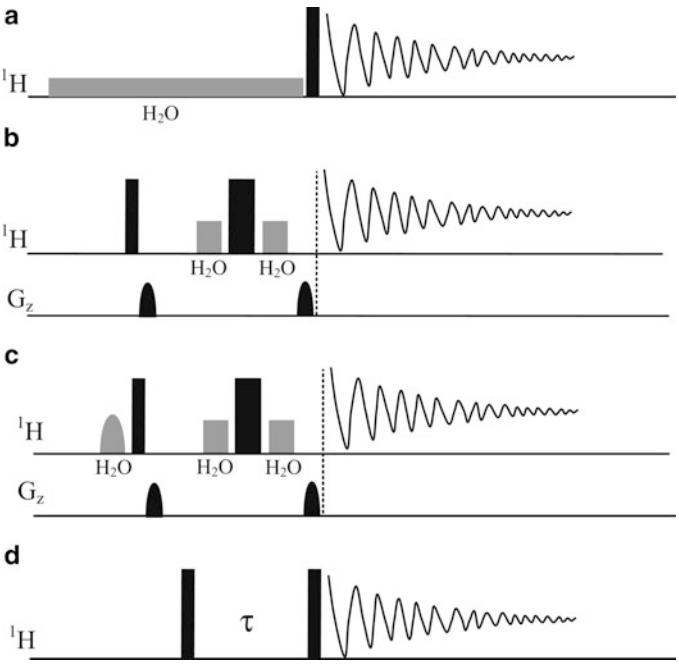

Fig. 4.14 Water suppression experiments. (**a**) PRESAT. Usually, the water saturation pulse is approximately 3 s. (**b**) WATERGATE. The 90° water selective pulses in gray can be shaped pulses (e.g., 3 ms sinc shape) or 1.7 ms rectangular pulses. (**c**) Water flip-back. The initial 90° water selective pulse is used to ensure water magnetization on the *z* axis after the hard 90° pulse to avoid radiation damping, which can be a 3 ms sinc or a 7.5 ms eburp1 shaped pulse. The two gradient pulses dephase and then refocus the solute magnetization, while the magnetization of residual water is continuously dephased by the gradient pulses because the pulse train formed by the two selective pulses sandwiching the hard 180° pulse keeps the water coherence order unchanged. The gradient strength is approximately 20 Gcm^{-1}. (**d**) Jump-return. The delay τ is set to $1/(4\Delta)$ in which Δ is the frequency difference between the water resonance and the center frequency of the interested region

magnetization approximately 10^4 greater than that from a type of protons in a protein. Therefore, the first task to do before acquiring data is to remove the solvent signal by a solvent suppression sequence. In the current section, some commonly used water suppression techniques are discussed.

4.8.1 Presaturation

There are various methods for water suppression, of which presaturation is the most basic and classical technique and is simple to use. A long and low power selective rectangular pulse is applied to saturate the water signal during the relaxation time (or predelay time) in the PRESAT pulse sequence shown in Fig. 4.14a.

Because the quality of the water saturation experiment depends greatly on the homogeneity of the magnetic field, the quality of shimming will substantially influence the result of the water suppression. In the experiment, the frequency of the long pulse is set on the water resonance to saturate the water proton population. Because the chemical shift of water is near the center of the ^{1}H chemical shift range, the carrier frequency is also placed on the water resonance though it can be set to any frequency within the spectrum. The pulse is set to longer than 3 s for a 1D experiment or to the longest time allowed for 2D experiments (usually 1.0–1.5 s). The pulse power must be set sufficiently low for important reasons, one of which is because the lower the power, the better the selectivity of the excitation. A high power will saturate signals in the region close to the water resonance. Additionally, for such a long pulse, the probe could be damaged if the pulse power were not sufficiently low. Usually, the pulse power is set in the range of 100–150 Hz, approximately 2 ms for the 90° pulse. For instance, the correct setting of the power should be attenuated about −48 dB from the power for a hard 90° pulse length of approximately 7 μs, which is typically in the range of −59 to −55 dB lower than the maximum pulse power of a 50 W ^{1}H amplifier. A typical setup procedure includes calibration of the 90° pulse, setting the carrier on the water resonance frequency and adjustment of the receiver gain. The hard pulse is calibrated first using a one-pulse sequence according to the procedure described in the calibration section. The carrier frequency offset is set to the water peak as described previously. After the receiver gain is adjusted using a single transient, the data are collected with the proper number of transients for the desired signal-to-noise ratio. Occasionally, a composite 90° pulse is used to replace the 90° pulse so as to minimize the effect of radiation damping (Chap. 2). It has also been noted that solvent signals originating outside the main sample volume (outside the probe coil) degrade the solvent suppression.

4.8.2 Watergate

The PRESAT is a simple method and is easy to set up. However, it reduces or partially saturates signals from exchangeable protons (amide protons) due to the rapid chemical exchange and spin diffusion between amide protons and saturated water protons and signals from protons resonating near the water resonance (α protons), causing partial saturation of H^{N} spins and reducing the intensity of amide protons (saturation transfer). The exchange rate of amide protons with water protons linearly increases with the pH value of the solution over a pH range of 3–9 (Connelly et al. 1992). To overcome this drawback, more sophisticated methods have been developed to perform water suppression without saturating the water magnetization.

The WATERGATE sequence (Piotto et al. 1992) shown in Fig. 4.14b is a popular technique used for water suppression of aqueous samples. It uses gradient pulses to dephase magnetization of both water and solute, and then to refocus only

the signals from the solute and further dephase the water magnetization. After the first hard 90° pulse brings the magnetization of all protons to the transverse plane, a 1 ms gradient pulse with an amplitude of approximate 20 Gcm^{-1} is applied to dephase the magnetization. The two 90° water selective pulses, which are either shaped or rectangular, are set on the water resonance. The net effect of the hard 180° pulse sandwiched by the two 90° water selective pulses is to keep the coherence order of water magnetization unchanged. Consequently, not only is the water magnetization dephased by the first gradient not refocused by the second, but the second gradient also further dephases the water magnetization. On the other hand, the second gradient refocuses the solute magnetization and produces a gradient echo because the hard 180° pulse changes the coherence order of the solute magnetization. The gradient echo used to dephase the water magnetization can sufficiently suppress water signal intensity compared to the presaturation method. However, it may still reduce the sensitivity of water exchangeable protons due to the partial saturation of water magnetization. Since the water magnetization is along the transverse plane at the time when acquisition starts, it needs much more time to completely relax back to its equilibrium state than do protein resonances due to its long T_1 relaxation time. Thus, the water will not fully relax back during the predelay time and will be partially saturated. The partial saturation will be transferred to the exchangeable protons by the saturation transfer, resulting in partial saturation of the H^N protons as reflected in a reduction of sensitivity for the desired resonances.

4.8.3 Water Flip-Back

An alternative version of Watergate, called water flip-back (Grzesiek and Bax 1993), uses a selective pulse on the water resonance before the Watergate sequence (Fig. 4.14c). The combination of the selective 90° and hard 90° brings the water magnetization back to the z axis before the first gradient pulse in the Watergate sequence. Because of the inhomogeneity of the 180° pulse, some magnetization from residual water is left on the transverse plane. The water flip-back sequence will suppress the magnetization from the residual water, whereas the majority of water magnetization stays on the z axis and is not disturbed to avoid radiation damping (Redfield et al. 1975). Consequently, the sensitivity for the exchangeable amide protons is increased because of the reduction of saturation transfer. Additionally, the amplitude of the required gradient pulses is considerably reduced to approximate 5 Gcm^{-1} for the gradient echo, which also increases the sensitivity of the experiment due to reduced effect of gradient pulses on the solute magnetization. In order to maximize the suppression of the water magnetization, the selective pulses must be well calibrated. To simplify the experimental setup, the flip-back selective pulse has a different shape and pulse length than the two Watergate selective pulses.

For instance, the first selective 90° pulse is a 90° eburp-1 pulse of 7.5 ms, whereas the last two can be either 1.7 ms rectangular 90° pulse or 3 ms sinc 90° pulses. The selective pulses are calibrated using the sequence described in the calibration section and the flip-back selective pulse is retuned in the water flip-back sequence by adjusting the fine power attenuation of the pulse.

In some experiments, distortion of the baseline occurs due to the fact that a substantial fraction of the FID is lost during the waiting time between the last pulse and acquisition (called the dead time). The time period is needed for the RF power of the high power pulse to go below the observable amplitude of the FID so the receiver is not saturated. A spin-echo sequence can be cooperated into any pulse sequence to prevent the FID from substantial loss during the dead time. The idea is to start the acquisition at the top of the first FID echo so that the full information of the FID can be retained. A typical value for the echo delays is 500 μs in the water suppression sequences, whereas the last delay is adjusted within 500 ± 50 μs to correct any phase errors in the spectrum.

4.8.4 Jump-Return

Although they provide sufficient water suppression, the gradient-based water suppression techniques and spin echo sequence may not produce observable signal for certain dilute samples because of partial loss in sensitivity during the experiment. For such samples, a better result can be achieved using the jump-return sequence shown in Fig. 4.14d (Plateau and Guéron 1982). The sequence is rather simple: a two-pulse sequence with two 90° pulses is separated by a delay. Like all other water suppression techniques, the carrier frequency is placed on the water resonance. The time of the delay is dependent on the spectral region of interest, which is determined by the frequency difference between the center of the region and the water resonance according to:

$$\tau = \frac{1}{4(\nu_c - \nu_w)} \tag{4.33}$$

in which ν_c is the center frequency of region of interest and ν_w is the water resonance. For example, the signals in the region of 7–10 ppm are expected to be observed. With the delay set to 111 μs for a 600 MHz spectrometer, the resonance at 8.5 ppm will precess 90° out of phase from the water resonance after the delay, whereas the water is on resonance. After the second 90° pulse that has a 180° phase shift from the first 90° pulse, the water is back to the z axis, whereas resonances in the region are detected with scaled intensity about the center frequency, ν_c. Normally, the second 90° pulse length is required to be optimized to achieve the best solvent suppression.

4.9 NMR Data Processing

For data analysis, an FID recorded during data acquisition is Fourier transformed to generate a spectrum. Prior to and post FT, the data are treated through a series of data processing steps to optimize sensitivity or resolution. A typical data processing includes DC offset correction (or drift correction), application of a solvent suppression filter, linear prediction, apodization, Fourier transformation, phase correction, and spectral baseline correction (if necessary).

4.9.1 DC Drift Correction

An FID collected by quadrature detection contains DC (direct current) offset error originating from the receiver. A DC offset in the time domain data produces a spike at the carrier frequency after Fourier transformation. The DC correction is automatically applied by NMR data processing programs without user's attention.

4.9.2 Solvent Suppression Filter

Although the water signal is suppressed during experiments, the suppression does not completely eliminate the unwanted water peak and sometimes the residual water signal is sufficiently high to interfere with nearby resonances. Digital filtering the FID will further suppress the water peak. There are two types of popular methods for solvent suppression by digital filtering, namely low frequency suppression and zero frequency suppression. In the low frequency method, a low passband digital filter with the desired bandwidth and resonance frequency on the water frequency is applied to the acquired FID (Marion et al. 1989a, b). The filter only allows the water signal and signals within the bandwidth of the filter to pass through. This filtered FID is subsequently subtracted from the original FID. Fourier transformation of the treated FID gives the water suppressed spectrum. The suppression filtering leaves a flat line in the bandwidth region if the profile of the digital filter fits the water line shape. Three parameters need to be specified for the filtering: the bandwidth in Hz (50–200 Hz), the resonance frequency position offset (in Hz) from the carrier frequency (the center of the spectrum) and the number of coefficients for the digital filter, which define the passband profile of the filter. More coefficients produce a digital filter with a steeper passband (brick wall type).

The zero frequency method first filters the FID using the same digital filtering as in the low frequency method. Then the filtered FID is fit with a polynomial function using a specified order. The polynomial is subtracted from the original FID to eliminate the water contribution to the FID. This method only subtracts the water signal residing exactly on resonance. The water peak is removed from the spectrum after Fourier transformation. In addition to the parameters used in low frequency

water suppression, the polynomial order needs to be specified, usually less than five. A brick wall type digital filter (with a higher number of coefficients) should be avoided in order to obtain reasonably fitting by the polynomial.

4.9.3 Linear Prediction

The first few points of the acquired time domain data are often distorted due to the imperfect condition of instrument hardware, such as tailing of RF pulses. Fourier transformation of the FID causes problems in the frequency domain such as baseline distortion. In addition, multidimensional data are always recorded with fewer points in the indirectly observed dimensions due to the long experimental time required. Collecting fewer data points in the indirectly observed dimension and more scans in the acquired dimension translates to higher S/N ratio for a given time. However, Fourier transformation of the truncated time domain data will severely distort the spectrum and reduce both sensitivity and resolution. Linear prediction is utilized to repair both types of FID distortions (Barkhuijsen et al. 1985). The algorithm analyzes the FID using the correct data points of the FID to obtain information on the frequencies present in the FID. Based on the analysis, it extrapolates more data points in the forward direction (forward prediction) to eliminate or reduce the truncation problem, or in the backward direction (back prediction) to replace the distorted initial points (in the observe dimension) or to extend a data point (in the indirect dimension). Mirror image linear prediction (Zhu and Bax 1990) uses the observed positive-time points to extrapolate negative-time points using the relationship of $f(-t) = f^*(t)$, in which * represents complex conjugation, resulting in doubling the size of the time-domain data points.

For the acquired dimension it may not be necessary to extend the data because it does not take long time to acquire the desired number of data points. However, backward prediction is sometimes used to correct the first few points that are influenced by the power of the last pulse. Forward predictions are always used for indirect dimensions because it provides more data points without actually acquiring the data so as to save experimental time (a more efficient way to acquire NMR data). The data points are usually doubled by the prediction (twofold prediction) because overextended data may introduce artifacts after Fourier transformation. The maximum number of points that can be used is the acquired data points for extending data points in either direction and the total data points minus the number of predicted points (usually the first one or two points) for replacing the distorted points in the backward predication.

4.9.4 Apodization

It is often necessary to manipulate time domain data (without altering frequencies) to improve the sensitivity or resolution of the spectrum. This can be achieved by the application of weighting functions. The basic idea is that according to the FT

similarity theorem, multiplying a FID by a function results in changing the shape of spectrum, but not the frequency:

$$F'(\omega) = H(\omega)F(\omega)$$
$$F'(\omega) = Ft\{h(t)f(t)\} = Ft\{f'(t)\} \tag{4.34}$$

in which $h(t)$ is a weighting function (or window function). The process used to change the appearance of the data is called data apodization. Because the FID trends to decay to zero, the S/N ratio (amplitude of FID to noise level) in the tail part of the FID is much lower than that at the beginning. By applying a weighting function that smoothes the tail region of the FID, the noise level can be zeroed out so that the sensitivity of the spectrum can be improved. The signals in the tail region, if any, will also be reduced to zero. An exponential function is used to serve this purpose:

$$h(t) = \mathrm{e}^{-t/a} \tag{4.35}$$

applying to the FID $f(t)$:

$$f(t) = \mathrm{e}^{-t/T_2} \tag{4.36}$$

results in new time-domain data $f'(t)$:

$$f'(t) = h(t)f(t) = (\mathrm{e}^{-t/a})(\mathrm{e}^{-t/T_2}) = \mathrm{e}^{-t/(T'_2)} \tag{4.37}$$

in which the apparent T'_2 is given by:

$$\frac{1}{T'_2} = \frac{1}{a} + \frac{1}{T_2} \tag{4.38}$$

This states that after Fourier transformation the line shape is broadened by the application of the exponential function with the line width increased by a factor of 2 (i.e., $T'_2 = T_2/2$) when $a = T_2$. Therefore, the exponential function decreases the resolution of the spectrum but increases sensitivity by removing the noise level at the tail of the FID. On the other hand, the sensitivity enhancement of the exponential function is reduced when the line broadening parameter a becomes larger. Exponential function is usually applied as a matched filter with $a = T_2$ which has a decay profile matched to the FID. Alternatively, if the exponential function can be applied with a negative a, the line width should be reduced as the reverse effect to the line broadening. The line shape of the spectral peak can be narrowed by a factor of 2 (i.e., $T'_2 = 2T_2$) when $a = -2T_2$. However, as its profile indicates, the function with a negative a amplifies the noise level at the end part of the FID and reduces the signal amplitude at the beginning part of FID, resulting in a significant loss in sensitivity. Resolution enhancement by applying these types of weighting functions will certainly degrade the sensitivity of the spectrum because the functions reduce the amplitude of the FID at the beginning. On the other hand, to increase sensitivity by smoothing the end part of FID, both signal and noise level are reduced and the

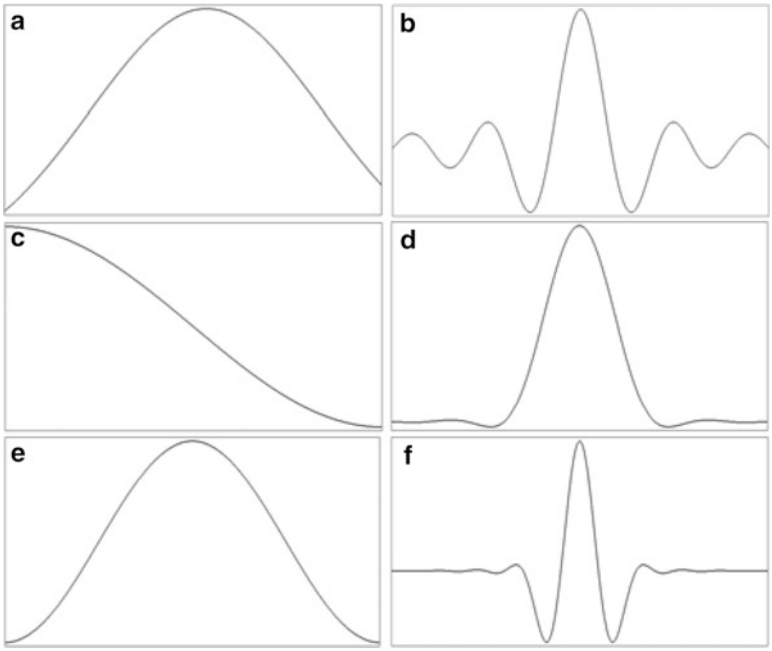

Fig. 4.15 Common weighting functions for apodization. (**a**) Lorentz–Gauss function with the parameters $a = -0.5$, $b = 1.5$, and (**b**) its Fourier transformation. (**c**) Squared 90° shifted sine bell function and (**e**) squared sine bell function, and their Fourier transformations (**d**) and (**f**), respectively

apparent T'_2 is decreased. As a consequence, the resolution of the spectrum is sacrificed. In general, sensitivity and resolution of an NMR spectrum cannot be improved simultaneously by means of applying a weighting function (or window function). Enhancement in one of the aspects has to be achieved at the expense of the other.

A usual solution to the problem is to combine the negative exponential function with another sensitivity enhancement function such as Gaussian function:

$$h(t) = \mathrm{e}^{-t/a}\mathrm{e}^{-t^2/b} \tag{4.39}$$

Compared to the natural line shape of NMR spectral peaks (Lorentzian line shape) with the same half height width, a Gaussian function has a much sharper line shape. While negative a gives resolution enhancement, b (always positive) provides sensitivity enhancement to compensate for the loss of sensitivity caused by a being less than zero. The optimization of parameters a and b of the Lorentz–Gauss function can increase resolution with a minimum loss of sensitivity and transforms the Lorentzian line shape to a narrow Gaussian line shape.

The Lorentz–Gauss function has a profile shown in Fig. 4.15 with the maximum in meddle of the function. This leads to the application of other functions with a similar profile but less reduction to the beginning of FID. Among them, the phase

shifted or unshifted sine-bell and squared sine-bell functions are commonly used for multidimensional data to achieve the desired sensitivity or resolution enhancement. Application of weighting functions such as Lorentz–Gauss, unshifted sine-bell, or unshifted squared sine-bell functions (Fig. 4.15) increases the amplitude of middle part, reduces the beginning, and smoothes the tail of the FID, producing an FID with longer decay (flatter FID). The corresponding spectral peak has a narrow line shape and hence the spectral resolution is increased. For 1D data, Lorentz–Gauss is commonly used if resolution needs to be improved, otherwise, an exponential function with $a = T_2$ is applied. For multidimensional data, an unshifted sine-bell or unshifted squared sine-bell function is utilized in the COSY to gain resolution enhancement, whereas the shifted weighting functions are used for all other 2D, 3D, and 4D data to improve the sensitivity. A 90°-shifted function provides maximum sensitivity enhancement.

4.9.5 Zero Filling

Data points collected in an FID are necessarily limited to just enough points to cover the FID to avoid collecting noise. However, a spectrum needs more data points to be able to characterize the individual peaks with the correct digital resolution. Digital resolution in the frequency domain is defined as SW/f_n, in which SW is the spectral window in Hz and f_n is the number of frequency domain points (a spectrum consists of f_n data points in the real part and f_n data points in the imaginary part). Additionally, $f_n = n_p/2$, in which n_p is the number of time domain points. By adding more points with zero amplitude to the end of the FID after data are collected (called zero-filling), the digital resolution is improved because f_n becomes larger after the zero-filling. The digital resolution without zero-filling is $SW/(½n_p) = 1/(DW \times n_p) = 1/at$, in which at is acquisition time and DW is dwell time.

Exchanging the order between apodization and zero-filling (i.e., the data are zero-filled first and then the apodization is applied) does not affect the result of the data processing because the amplitudes of the zero-filled data points are still zero after the apodization. However, the apodization after the zero-filling takes more computing time. Although this extra computing time is unnoticeable in 1D and 2D data processing, it may be substantial during 3D and 4D data processing. Therefore, the apodization is usually applied before zero-filling.

4.9.6 Phase Correction

Fourier transformation of an FID gives a spectrum which can be represented by:

$$F(\omega) = \mathrm{R}(\omega)\cos(\theta) + \mathrm{I}(\omega)\sin(\theta) \tag{4.40}$$

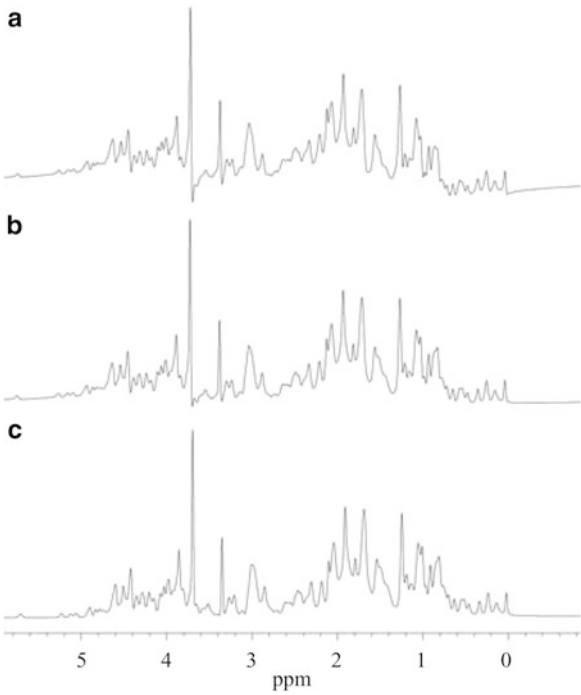

Fig. 4.16 Phase correction of spectrum. (**a**) The spectrum contains a zero order phase error of 40°. All peaks are distorted by the same amount. (**b**) The spectrum contains a first order phase error of 40°. The degree of distortion of the spectrum is frequency dependent and peaks at downfield are off more than those in the upfield region. (**c**) Spectrum with correct phase

in which R and I are the real and imaginary parts of the spectrum $F(\omega)$, respectively, and θ is the phase error of the spectrum. Ideally, $\theta = 0$, that is, real part is pure absorption and the imaginary part is pure dispersion. In practice, $\theta \neq 0$ for most cases, because the FID does not start with the maximum amplitude. There are many factors causing the problem, one of which is that quadrature detection has a phase error and does not acquire pure cosine and sine components of the FID. This causes an equal amount of phase error on all resonances of the spectrum and is called zero order phase error (Fig. 4.16a). The other type is first order phase error typically introduced by the delay between the end of last pulse and the start of acquisition (dead time, or receiver gating time). This delay is unavoidable because of tailing problem of the RF pulse. During the dead time, the amplitudes of time domain signals with different frequencies are reduced by different fractions, leading to a frequency-dependent phase error (Fig. 4.16b). The total phase error is the linear combination of the two types of phase errors:

$$\theta(\omega) = \phi_0 + (\omega - \omega_0)\phi_1 \tag{4.41}$$

in which ϕ_0 and ϕ_1 are the zero order and first order phase error, respectively, and can be corrected by the phase correction function of a data processing programs.

It should be noted that an experiment can be set up in such a way that the FID is acquired without any phase error (both ϕ_0 and ϕ_1 are zero). Adjusting the dead time to ensure all signals start at a maximum amplitude eliminates the first order phase error.

Table 4.2 Methods of quadrature detection in the indirect dimension

Methods	DW	Exp. per incr.	Phase shift	τ	Phase correction	References
States	1/SW	2	90° for same incr. 0° per incr.	DW/2	90°, −180°	States et al. (1982)
TPPI	1/(2 × SW)	1	90° per incr.	DW	90°, 0°	Marion and Wuthrich (1983)
States-TPPI	1/SW	2	90° for same incr. 90° per incr.	DW/2	90°, −180°	Marion et al. (1989a, b)

This can be done by simply optimizing the dead time to the point that the first order phase error is zero, which is usually longer than the value set by the instrument software (rof2 and alfa on an Agilent spectrometer, de on a Bruker spectrometer). The drawback is loss in sensitivity if the delay is long. Alternatively, in a better method, a spin echo sequence is used during the normal delay period which refocuses all coherence at any desired time so that the FID is always starts with the maximum amplitude. The zero order phase error can be corrected by setting the receiver phase after the first order phase error is eliminated in the above procedure. The adjustment of the receiver phase can be done by the spectrometer software or by adding an adjustable phase parameter to the receiver phase table in the pulse sequence. Note that every time probe tuning is adjusted, zero-order phase is changed. After the above adjustment of both zero order and first order phases, the acquired FID does not contain any phase error. Therefore, phase correction after Fourier transformation is not necessary.

The phase error for the indirect dimension can be corrected after the t_1 Fourier transformation (see the following section). However, the first order phase error in the indirect dimension causes such problems as baseline distortion and dispersive folded cross-peaks, which significantly degrade the sensitivity of the spectrum. To avoid these problems, the phases can be set before the acquisition according to the relationships:

$$\begin{aligned} \phi_1 &= -\tau \times \mathrm{SW} \times 360^\circ \\ \phi_0 &= -\frac{1}{2}\phi_1 \end{aligned} \tag{4.42}$$

in which SW is the spectral window of the indirect dimension, and τ is the sampling delay, which is the sum of all delays and 180° pulses in the evolution time. The 90° pulses that flank the evolution time are also included in the sampling delay in terms of the 90° pulse length multiplied by $2/\pi$. The sampling delay τ is set to $\tau = 0$ or $\tau = \mathrm{DW}/2$ (DW is the dwell time of the indirect dimension. See Table 4.2 for the relationship between SW and DW in the t_1 dimension), resulting in $\phi_0 = 0^\circ$, $\phi_1 = 0^\circ$ for $\tau = 0$, and $\phi_0 = 90^\circ$ and $\phi_1 = -180^\circ$ for $\tau = 1/(2\ \mathrm{SW})$.

The conditions can be met by adjusting the initial value of t_1 as described in the following pulse sequence elements:

(a) Homonuclear evolution period $90°-t_1-90°$
The sampling delay is given by:

$$\tau = t_1(0) + \frac{4 \times \mathrm{pw}_{90}}{\pi} = \frac{\mathrm{DW}}{2} \quad \text{for } \phi_0 = 90° \text{ and } \phi_1 = -180° \tag{4.43}$$

The initial t_1 value is calculated according to:

$$t_1(0) = \frac{\mathrm{DW}}{2} - \frac{4 \times \mathrm{pw}_{90}}{\pi} \tag{4.44}$$

in which $t_1(0)$ is the initial value of t_1, and pw_{90} is the 90 pulse length. The effect of the phase variation during the flanking 90° pulses can be removed from the sampling delay in the pulse sequence element $90° - t_1 - \delta - 180° - \delta - 90°$, in which δ is a fixed delay. Because the 180° pulse is placed symmetrically in the initial evolution period ($t_1 = 0$) and refocuses the effect of the phase variation, the sampling delay is zero. Consequently, $t_1(0)$ can be set to $t_1(0) = \mathrm{DW}/2$ or $t_1(0) = 0$. For $t_1(0) = 0$, the first point of the interferogram is usually scaled by a factor of 0.5 prior to Fourier transformation (Otting et al. 1986).

(b) HMQC element

- With spin decoupling $90°(\mathrm{X}) - ½t_1 - 180°(^1\mathrm{H}) - ½t_1 - 90°(\mathrm{X})$
The sampling delay is given by:

$$\tau = t_1(0) + \mathrm{pw}_{180(^1\mathrm{H})} + \frac{4 \times \mathrm{pw}_{90(\mathrm{X})}}{\pi} = \frac{\mathrm{DW}}{2} \tag{4.45}$$

$$t_1(0) = \frac{\mathrm{DW}}{2} - \mathrm{pw}_{180(^1\mathrm{H})} - \frac{4 \times \mathrm{pw}_{90(\mathrm{X})}}{\pi} \tag{4.46}$$

in which $\mathrm{pw}_{180(^1\mathrm{H})}$ and $\mathrm{pw}_{90(\mathrm{X})}$ are the pulse lengths of a ^{1}H 180° pulse and a heteronuclear 90° pulse, respectively.
- Without spin decoupling $90°(\mathrm{X}) - t_1 - 90°(\mathrm{X})$
The initial $t_1(0)$ is set to:

$$t_1(0) = \frac{\mathrm{DW}}{2} - \frac{4 \times \mathrm{pw}_{90(\mathrm{X})}}{\pi} \tag{4.47}$$

- Constant time $90°-½t_1 - T - 180° - (T - ½t_1) - 90°$.
Because the refocusing 180° pulse is placed symmetrically in the initial evolution period ($t_1 = 0$), the sampling delay is zero. As mentioned earlier, $t_1(0)$ can be set to either DW/2 or zero.

4.10 Two-Dimensional Experiments

4.10.1 The Second Dimension

The signals of protons in a protein sample recorded in 1D NMR experiments are not able to be completely assigned due to severe overlapping of the signals. To improve the resolution for spectral assignment, a second frequency dimension is introduced to disperse the signals over two frequency dimensions, forming a 2D NMR spectrum. In a 1D experiment, the FID is acquired after an RF pulse or pulses (called the preparation period). In a 2D experiment, one additional period called the evolution time, which contains a variable time delay t_1, is introduced into the experiment between the preparation and acquisition periods (Fig. 4.17). The evolution delay increases systematically by the same amount of time for each increment during a 2D experiment from zero to the final value determined by the number of increments. An FID is acquired for one increment with the starting value of the t_1 evolution time. For next increment, an FID is acquired with an increased t_1 and all other parameters the same as the previous FID, and so on for the required number of increments. After the experiment is done, all the FIDs are transformed with the same phase parameters. The phase of the signals after Fourier transformation is modulated as a function of the t_1 evolution time. As a result, the amplitudes of the signals after Fourier transformation vary sinusoidally as a function of the t_1 evolution time, which forms an interferogram similar to a FID when the

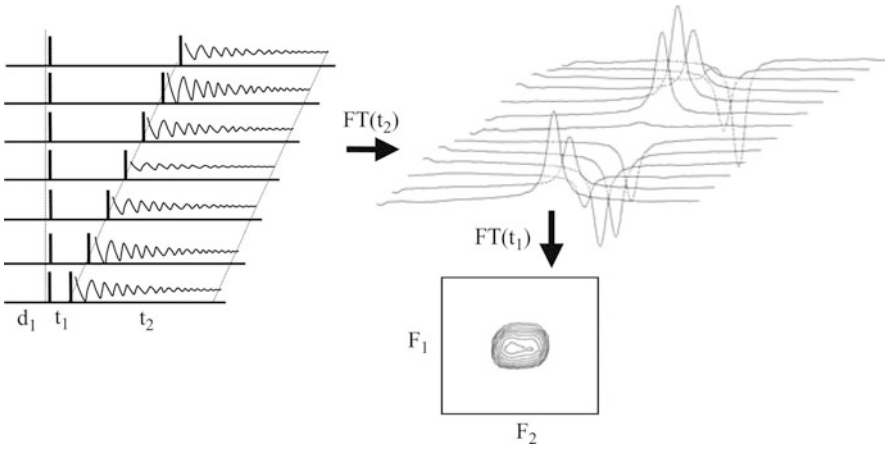

Fig. 4.17 Two-dimensional experiment and 2D spectrum. The evolution time t_1 is increased systematically for each of the FIDs. The FIDs acquired during t_2 are Fourier transformed to obtain a set of 1D spectra. The second Fourier transformation is applied along t_1, that is, each point of the spectra, resulting in a cross peak coordinated by both frequencies on F_2 and F_1. The F_2 dimension has better digital resolution because t_2 is always longer than t_1. The parameter d_1 is the relaxation delay (or predelay) and t_2 is the acquisition time

amplitude of a peak is plotted as a function of t_1 (Fig. 4.17). Fourier transformation of the second FID obtained by the t_1 evolution time generates another frequency domain as the transformation of the acquired FIDs. The result of the two Fourier transformations is a 2D NMR spectrum with two frequency axes and an intensity axis on the third dimension that is usually plotted as contours. The second dimension can be frequency for ^{1}H, which gives a square spectrum with diagonal peaks, or a heteronucleus which gives an asymmetric spectrum. Two dimensional experiments will also contain other periods in addition to the evolution time such as a mixing period. However, it is the evolution time that introduces the additional dimension into a spectrum. Similarly, more dimensions can be formed by introducing additional evolution time periods. The widely accepted terminology is that for nD data, $t_1, \ldots, t_{n-1}$ are evolution delays, and t_n is the acquisition period, whereas $F_1, \ldots, F_{n-1}$ are the indirect dimensions generated by the corresponding evolution times and F_n is the direct dimension from the observed FID. For instance, in a 3D spectrum the F_3 dimension is obtained from the transformation of the observed FID or t_3, which is the direct dimension, whereas the F_1 and F_2 dimensions are from the evolution times t_1 and t_2, respectively, and hence the indirect dimensions.

Before setting up a 2D experiment, calibrations of pulses, water resonance frequency, and optimization of the spectral window should first be performed. The spectral window is set to the value optimized in the 1D spectrum. The acquisition is generally set to about 200 ms for homonuclear experiments or 64 ms for heteronuclear experiments with ^{15}N or ^{13}C decoupling during acquisition. If each FID is acquired with the number of points, n_p and number of increment is n_i, the final size of the data file is $n_p \times n_i$. Assuming that each transient of a FID takes n seconds to finish (n is called the recycle time) and n_t transients are taken for each FID with n_i increments, the total experiment time will be $n_t \times n \times n_i$. A 2D experiment can take as little time as 2–15 min to finish (e.g., gCOSY, gHSQC). Instrument software can be used to calculate the total experiment time before hand.

4.10.2 Quadrature Detection in the Indirect Dimension

In order to correct the phase distortion of cross peaks, quadrature detection in the indirect dimension is necessary to obtain a phase sensitive 2D spectrum. This is achieved by hypercomplex or TPPI methods similar to quadrature detection in the observed dimension (see Sect. 2.4). In the hypercomplex method (also known as the States method; States et al. 1982), two FIDs are recorded for each t_1 increment. In the second FID, the phase of the preparation pulse or pulses (the pulse or pulses prior to the t_1 evolution period) shifts by 90° phase (Fig. 4.18). Two sets of data are obtained: one with 0° phase and the other with 90° phase. After the first Fourier transformation, the t_1 interferogram is constructed by taking the real part of the 0°-phase data (open circles in Fig. 4.18) as the real part of the interferogram, and the real part of the 90°-phase data (filled circles) as the imaginary part of the interferogram.

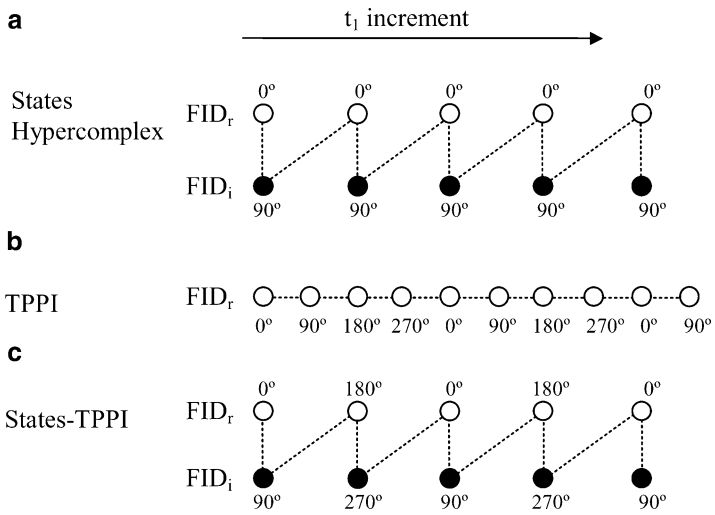

Fig. 4.18 Quadrature detection methods in the indirect dimension. Each *circle* represents an FID: the *open circles* represent the FIDs used for the real part (FID_r) of the t_1 interferogram. The *filled circles* represent the FIDs used for the imaginary part (FID_i) of the t_1 interferogram. The values above or below the circles represent the relative phases of the pulse (or pulses) before the t_1 evolution period in a pulse sequence. The *dotted lines* represent the order of FIDs being acquired. (**a**) The States or hypercomplex method. For each t_1 increment, two FIDs are acquired. After t_2 Fourier transformation (FT), the real parts of the open-circled FIDs form the real part of the t_1 interferogram and the real parts of the filled FIDs form the imaginary part of the t_1 interferogram. Complex FT is then applied to transform t_1 to the F_1 dimension. (**b**) TPPI method. The t_1 is incremented for every FID along with a 90° shift of the relative phase of the pulse (or pulses) before the t_1 evolution period. The real parts of the FIDs form the real part of the t_1 interferogram, which is then transformed by a real Fourier transformation. (**c**) States-TPPI method. The data are acquired in the same way as the States method except the relative phase is increased by 90° after each FID is acquired. As a result, the axial peaks are suppressed by shifting them to the edge of the spectrum. Complex FT is used in both dimensions

Therefore, both parts of the interferogram are from absorptive data. A phase sensitive spectrum is obtained after the interferogram is transformed by the complex Fourier transformation. The t_1 increment is set to $1/(2 \times SW_1)$, in which SW_1 is the spectral window in the F_1 dimension.

In the TPPI method (Fig. 4.18b; Marion and Wuthrich 1983), the phase of the preparation pulse shifts 90° for every t_1 increment. After the first Fourier transformation, the t_1 interferogram is constructed by taking the real part of all FIDs as real part and the interferogram is transformed by the real Fourier transformation, resulting in a phase sensitive spectrum. Similar to the sequential acquisition method, the TPPI method requires twice as fast t_1 increment as the hypercomplex method. Therefore, the t_1 increment is set to the $1/SW_1$. The advantage of TPPI relative to the hypercomplex method is that axial peaks appear at the edge of F_1 dimension ($F_1 = 0$), whereas axial peaks are located in the center of the 2D spectrum with the States method, which overlap with the signals of interest.

However, TPPI has the disadvantage of undesirable folding properties (Marion and Bax 1988). To overcome this disadvantage while still suppressing the axial peaks, a combination of the States and TPPI methods was developed (Marion et al. 1989a, b).

The States-TPPI method combines the two methods together as shown in Fig. 4.18c. The data are acquired in the same way as the States method except that the phase of the preparation pulse shifts 90° after each FID is acquired. As a result, the axial peaks are suppressed and the spectrum does not have the TPPI folding properties. The t_1 increment is set to $1/(2 \times \mathrm{SW}_1)$, the same as in the States method. Complex Fourier transformations are used in both dimensions.

4.10.3 Selection of Coherence Transfer Pathways

When quadrature detection is used, only coherence with the order of either +1 or −1 can be observed (single quantum coherence), but not both at the same time. The common choice assumes that the coherence order of −1 is observed in all experiments by quadrature detection. An initial non-90° pulse generates higher order coherence in addition to the single quantum coherence. Therefore, there exist many other coherence transfer pathways along with the desired pathway at the end of a pulse sequence, which produce observable signals during acquisition time. To select the specific coherence transfer pathway and eliminate the unwanted signals from the other pathways, either phase cycling or gradient pulses are usually utilized.

The change in the phase of the coherence caused by an RF pulse or gradient pulse depends on its coherence order p. The selection of the coherence pathway is based on this property of the coherence phase. Phase cycling uses changes in the phase of RF pulses which lead to different phase shifts of the coherence. If the phase of an RF pulse is set to ϕ, the phase shift gained by the coherence experiencing a coherence order change Δp by the pulse is given by $-\phi\Delta p$. A particular coherence transfer pathway can be selected by phase cycling using N steps with increments of $\phi = 360°/N$. Phase cycling is the process in which the phases of pulses in a pulse sequence are shifted after each acquisition during the signal averaging (detailed treatment of phase cycling methodologies can be found in Bodenhausen et al. 1984; Bain 1984). The pathway selection by phase cycling requires precise phase shifts of RF pulses and repeated acquisitions with different phase shifts of pulses. Usually, it is not the method of choice. Coherence selection by gradient pulses is more commonly used in multidimensional NMR experiments to reduce experimental time in addition to other advantages.

The coherence selection by gradient pulses is achieved by applying a gradient pulse to dephase and then refocus a specific coherence, while allowing the unwanted coherence to continue dephased. Unlike the phase cycling method, phase changes by gradient pulses only depend on the coherence order at the time the gradient pulse is applied, not the difference of two coherence orders.

The spatially dependent phase induced by a gradient pulse with field strength G applied on a coherence of order p for a duration τ is given by:

$$\phi = G\tau\gamma p \tag{4.48}$$

in which γ is the gyromagnetic ratio of nuclear isotope. In the case of a heteronuclear system and a shaped gradient, the phase is described by:

$$\phi = sG\tau\gamma p \tag{4.49}$$

in which s is the shape factor that describes the amplitude profile of gradient pulse.

Considering a pair of simple dephasing-refocusing gradient pulses to select a specific homonuclear coherence transfer pathway from p_1 to p_2, the dephasing gradient pulse of duration τ_1 prior to the RF pulse induces a phase of coherence with order p:

$$\phi_1 = s_1 G_1 \tau_1 p_1 \tag{4.50}$$

Similarly, the refocusing gradient pulse of duration τ_2 following the pulse generates a phase:

$$\phi_2 = s_2 G_2 \tau_2 p_2 \tag{4.51}$$

The condition for the selected coherence to be refocused at the end of the refocusing gradient pulse is that the overall phase change ($\phi_1 + \phi_2$) after the gradient pulses becomes zero. Because usually the gradient pulses are applied with the same shape in a pulse sequence, the shape factor s may only be different by the sign of the gradient, + or −. For the use of two gradient pulses, the selection condition can be rearranged as:

$$s_1 G_1 \tau_1 p_1 = -s_2 G_2 \tau_2 p_2 \tag{4.52}$$

This states that the desired coherence transfer pathway is achieved by adjusting the duration, amplitude and the sign of the gradient pulses and the unwanted pathways can be removed when the condition is not met for other coherences, provided the amplitude of the gradient pulses is sufficiently high to completely dephase the unwanted coherences.

When more than two gradient pulses are used for the coherence selection, the refocusing condition is also the same that the overall phase induced by all gradients for the selected pathway is zero:

$$\sum_i \phi_i = \sum_i s_i G_i \tau_i p_i = 0 \tag{4.53}$$

This condition applies to all combinations of gradients used in the coherence selection. When more than two gradients used, the combination for dephasing

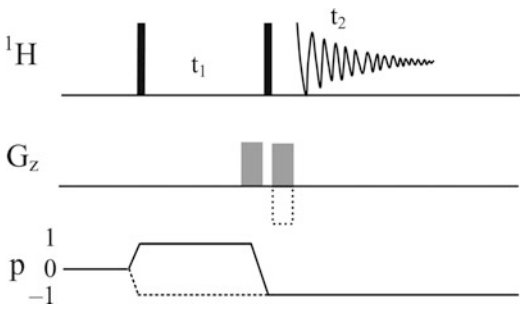

Fig. 4.19 COSY pulse sequence with coherence transfer pathway diagram. The general points for coherence selection using coherence transfer pathway are described as follows. The coherence transfer pathway must start at the equilibrium state in which the magnetization is along the field direction, z magnetization, represented by coherence order of $p = 0$. The first pulse acting on the equilibrium z magnetization gives rise to only single quantum coherence $p = \pm 1$. Delays without an RF field do not change the coherence order. Finally, the pathway must terminate at $p = -1$ as quadrature detection is used to observe the complex signals. The *solid line* in the coherence transfer pathway diagram and the solid gradient represents N-type selection, whereas the *dotted* coherence pathway and the open gradient is P-type selection

and refocusing can be different. For instance, the coherence can be continuously dephased by many gradients until the final gradient right before acquisition refocuses the desired coherence. Alternatively, the set of gradients can be used to select one part of the preferred pathway, whereas others select the other part of the pathway. More examples are discussed in detail for 2D experiments in the following sections.

4.10.4 COSY

Shown in Fig. 4.19 is the gradient version of the 2D *Co*rrelation *S*pectroscop*y* experiment, abbreviated as COSY, which is one of the earliest 2D experiments. It has the simplest 2D pulse sequence consisting of two 90° pulses separated by the evolution time, t_1. The first 90° pulse rotates the equilibrium magnetization to the transverse plane and generates single-quantum coherence. During the evolution time t_1, the single-quantum coherence evolves, resulting in F_1 frequency labeling of the detected coherence. The last pulse transfers the magnetizations between spins via the scalar coupling between them. Finally, the correlated coherence is detected as the FID. The coherence selection is achieved by the gradients pulses following each RF pulse.

There are two possible pathways for acquiring COSY spectra, as shown in Fig. 4.19. A pathway through $p = -1$ is known as P-type (or anti-echo) in contract to that through $p = +1$ known as N-type (echo). The frequency modulations of the coherence during t_1 and t_2 have the same sign for the P-type pathway, whereas they have opposite sign for the N-type pathway. The N-type COSY is recorded using the

last gradient with the same sign as the first one because the refocusing condition is obtained by $G_1p_1 = -G_2p_2$, in which $p_1 = 1$ and $p_2 = -1$, assuming that both gradient pulses have the same amplitude, shape, and duration. The P-type spectra can be similarly obtained by setting the refocusing gradient pulse with the sign opposite to the first one with the same duration and amplitude. The selection of either the N- or P-type pathway by gradient pulses results in frequency discrimination in the F_1 dimension without using any of the quadrature detection methods. However, the two pathways are not usually selected simultaneously.

Both pathways give rise to phase-twisted line shapes containing the superposition of absorptive and dispersive signals, which is caused by the use of the gradient during the evolution period. A phase sensitive spectrum can be constructed by acquiring both types of data separately and then combining them in such a way that the axis-reversed N-type spectrum is added to P-type. In the resulting spectrum, the dispersive portion due to the phase twist is canceled and complete absorptive line shapes are obtained (see quadrature detection in the indirect dimension). The phase sensitive spectrum acquired by this method has a reduction in sensitivity by a factor of $2^{1/2}$ compared to that by States, States-TPPI or TPPI methods due to the cancelation of the absorptive and dispersive signals. Alternatively, N-type and P-type data can be combined in a different way to obtain a phase sensitive spectrum. Addition of the two data sets generates cosine-modulated data, whereas subtraction of the two yields sine-function data. Hypercomplex data are formed by using the constructed cosine and sine portion of the data, which can be processed in the same way as the States method.

Digital resolution in the F_1 dimension also has a great influence on the sensitivity of the COSY spectrum owing to the antiphase character of the cross peaks. Because the cross peaks contain scalar coupling, the last t_1 increment must have a t_1 value ($t_{1,\max}$) greater than $1/(4J)$, whereas t_2 is set to a value comparable to $1/(2J)$. Usually, $t_{1,\max}$ is chosen in the range of 50–80 ms and t_2 is approximately 200 ms. For example, the data collected with 2,048 complex points and 600 increments yields $t_{1,\max}$ of 50 ms and t_2 of 170 ms for spectral window of 10 ppm on a 600 MHz instruments. Linear predication is used to add sufficient data points for both the F_1 and F_2 dimensions.

4.10.5 DQF COSY

The double quantum filtered (DQF) COSY is sometimes preferred over the COSY experiment because the intense peaks from uncoupled singlets are substantially attenuated and resolution in the region adjacent to the diagonal peaks is dramatically improved. The advantages of DQF COSY also include correction of the phase distortion present in COSY and absorptive line shapes for both cross peaks and diagonal peaks. The drawback of DQF COSY is reduction in sensitivity, thus requiring longer experimental time. The basic pulse sequence of DQF COSY consists of three 90° pulses (Fig. 4.20). The single quantum coherence generated

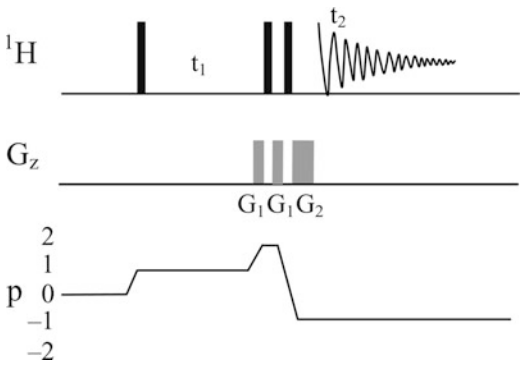

Fig. 4.20 Double-quantum filtered COSY pulse sequence with coherence transfer pathway diagram. The RF pulses are 90° pulses. The double-quantum coherence is selected by the second gradient with the coherence order $p_2 = 2$. The ratio of the gradients is $G_2 = 3G_1$. The N-type coherence pathway is shown in the coherence transfer pathway diagram

by the 90° pulse evolves during t_1. After the second 90° pulse transfers the coherence into double quantum coherence, the last 90° pulse produces observable single quantum coherence. Only double quantum coherence will be selected by the gradient pulses. The last gradient pulse refocuses the double quantum coherence dephased by the first two gradient pulses, leaving other coherence to continue dephased. According to the selection rules, the overall phase created by the gradient pulses must be zero. Assuming that the gradient pulses have the same duration, then

$$p_1G_1 + p_2G_2 + p_3G_3 = 1G_1 + 2G_1 - 1G_2 = 0 \tag{4.54}$$

$$G_2 = 3G_1 \tag{4.55}$$

The spectrum may contain phase errors caused by the application of the gradient pulse during t_1 evolution. Higher order multiquantum filter experiments can also be implemented using the coherence selection rule. For instance, the detectable triple quantum filtered coherence is refocused by the condition:

$$G_1 + 3G_1 - 1G_2 = 0 \tag{4.56}$$

$$G_2 = 4G_1 \tag{4.57}$$

The above selection of double quantum coherence chooses the N-type coherence pathway ($p = +2$), whereas the P-type pathway with $p = -2$ is not selected by the gradient pulses. As a result, half of the initial magnetization does not contribute to the detected magnetization, causing a loss of signal compared to the data acquired by the phase cycling method. An absorption mode spectrum can be obtained by acquiring P- and N-type data and then combining the data as

described above. States or States-TPPI quadrature detection methods can also be employed to obtain quadrature detection in the F_1 dimension and thus produce pure absorption spectra.

4.10.6 TOCSY

In a 1D ^{1}H spectrum of a protein, the side chain region (up-field region) is very crowded with severe spectral overlap due to the large number of side chain protons. In the contrast, the chemical shifts of H^N protons are less crowded, especially for small proteins, and the peaks are sometimes well resolved. It is useful in resonance assignment to transfer the correlations of side chain protons to the region of H^N proton chemical shifts. TOCSY (also known as HOHAHA; Braunschweiler and Ernst 1983; Bax and Davis 1985a, b) experiments were developed to obtain, through coherence transfer via ^3J scalar couplings, the relayed correlations between spins within a spin system, a network of mutually coupled spins. COSY experiments provide the information about the correlation between spins, whereas TOCSY transfers the coherence to other coupled spins through the ^3J coupling (through molecular bonds) by isotropic mixing. During the mixing period, the coherence along an axis on xy plane is transferred throughout the spin system under the interaction of scalar coupling, at the same time the multiquantum coherence is dephased by the inhomogeneity of RF pulses in the isotropic mixing pulse train. Several methods for the isotropic mixing have been used in different types of TOCSY experiments (Sect. 4.5.2). Much effort has been spent on the development of mixing pulse sequences (also known as spin lock sequences) that use minimal RF power to produce wide isotropic frequency ranges. DIPSI series mixing sequences are most commonly used now, among others such as Mlev17, Waltz16, and clean-TOCSY.

During the mixing time, the magnetization of amide protons is transferred to other protons within amino acid residues through three-bond scalar coupling. Because there is no through-bond scalar coupling between the interresidual amide proton H^N and α proton H^α, the magnetization cannot be transferred across the peptide bond. The transfer distance (the number of protons the H^N magnetization can reach) depends on the efficiency of the spin lock sequence, length of mixing time, the coupling constants, and the relaxation rate of the molecule. Protons further away from the H^N proton require a longer mixing time to reach. Ideally, it is preferred to obtain magnetization transfer to every proton within the spin system. However, it is practically difficult to acquire a single TOCSY with a mixing time to optimize magnetization transfer from H^N to all other protons. The magnitude of transfer to neighboring protons decreases quickly as the mixing time exceeds than 30 ms. For remote protons, the magnetization transfer is achieved with the mixing time as long as 100 ms. The correlations between H^N and H^α, H^β can be observed in a TOCSY with a mixing time of 30 ms, whereas a 60 ms or longer mixing time is required to achieve magnetization transfer from H^N to other side chain protons. Normally, a TOCSY experiment is first acquired with a mixing time in the range of 30–60 ms to

efficiently transfer H^N magnetization to the neighboring side chain protons. Then, the experiment is repeated with a longer mixing time to favor the long range magnetization transfer of H^N magnetization to the end protons of the side chain, but is usually less than 100 ms to avoid magnetization loss caused by relaxation.

TOCSY data are collected in a phase sensitive mode in the F_1 dimension, for example. States-TPPI, with 512 increments which yield 256 complex points in the F_1 dimension. Trim pulses are normally set to 2 ms. The pulse length of spin lock is dependent on the spectral window of the 2D data. Usually, a 90° spin lock pulse is about 25–30 μs, which covers a bandwidth close to 8–10 kHz, and a 90° excitation pulse is less than 10 μs. It creates sample heating problem when 90° spin lock pulse is shorter than 20 μs. The problem becomes severe for short 90° spin lock pulses in the case of the clean TOCSY. A spin lock time in the range of 30–60 ms is required for protein samples, which can only be selected in an integer number of spin lock cycles. A typical set up involves calibrating a 90° pulse at high power, a 90° spin lock pulse at lower power, and optimizing the spectral window. After the data are acquired with 200 or more FIDs, linear prediction should be utilized to double data points for the F_1 dimension. TOCSY data are processed with a square sine-bell function shifted by 30–60° before Fourier transformation. Note that spin lock power can be calculated based on the power and length of hard 90° pulse within the linear range of the RF amplifier.

4.10.7 NOESY and ROESY

COSY and TOCSY use scalar coupling (through bond nuclear interaction) to correlate the spins within a spin system. These types of experiments provide orientational information about the molecules via three-bond J coupling in addition to the correlation used in resonance assignment. The through-space nuclear interaction (dipolar interaction) is also used in multidimensional experiments to obtain distance information between spins for structural and dynamic studies of molecules. NOESY (nuclear Overhauser effect spectroscopy) and ROESY (rotating frame Overhauser effect spectroscopy, also known as CAMELSPIN for cross-relaxation appropriate for minimolecules emulated by locked spins) experiments utilize the dipolar interaction in the form of cross-relaxation to correlate spins that are close in distance (Bothner-By et al. 1984; Bax and Davis 1985a, b; Griesinger and Ernest 1987).

During the mixing time τ_m of the pulse sequences shown in Fig. 4.21b, c correlations between spins that are close in space occur via cross-relaxation, which give rise to cross peaks in NOESY and ROESY spectra. In a NOESY experiment, the intensities of the cross peaks not only are proportional to the cross-relaxation rate but also come from spin diffusion. Although the contributions to the cross-peak intensity from both mechanisms increase as the mixing time τ_m increases, the spin diffusion effect can be minimized with a short mixing time. For protein samples, the mixing time is usually chosen in the range of 30–200 ms to avoid the spin diffusion effect. For a quantitative measurement of the internuclear

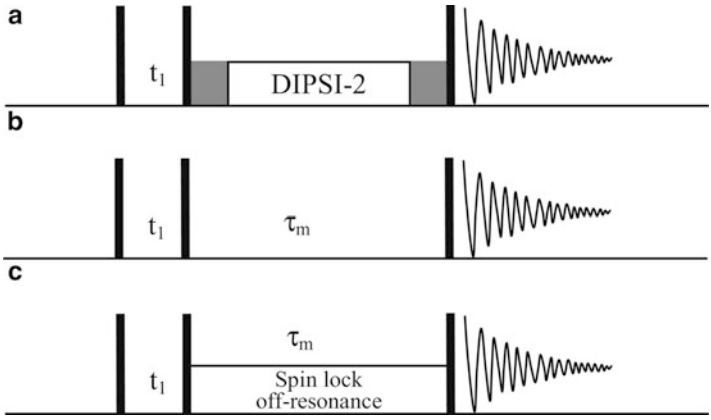

Fig. 4.21 Two-dimensional homonuclear pulse sequences. (**a**) In TOCSY, a DIPSI-2 pulse train is applied with low power during spin lock period. The trim pulses (*gray bars*) are usually set to 2 ms. (**b**) τ_m is the mixing time in the NOESY sequence. (**c**) Spin lock pulses during the mixing time τ_m in the ROESY experiment are set to off-resonance to avoid the generation of TOCSY cross-peaks that have an opposite sign to the ROESY cross-peaks. *Solid bars* represent 90° pulses

distance, a series of NOESY experiments with different mixing times is collected and an NOE buildup curve is obtained by plotting the cross-peak intensity vs. the mixing time for each individual resonance. The NOESY cross-peak intensity (or volume) is proportional to the length of the mixing time:

$$I_a = \xi \frac{\tau_m}{r_{ab}^6} \tag{4.58}$$

in which ξ is a constant for a given sample at a specific magnetic field strength, τ_m is the mixing time, and r_{ab} is the distance between protons a and b. The initial linear range of the NOE buildup curve is used to calibrate and calculate the distance based on the cross-peak intensity relative to the intensity from a known distance. The constant ξ is first obtained by measuring the cross-peak intensity of a NOESY spectrum with a short mixing time for a known internuclear distance:

$$\xi = I_{ref} \frac{r_{ref}^6}{\tau_m} \tag{4.59}$$

in which I_{ref} is the cross-peak intensity of a reference proton to another proton with a fixed and known distance r_{ref}. ξ is used to calculate the distance r_{ab} from I_a for all cross peaks. Alternatively, the cross-peak intensity I_{ref} from r_{ref} can be used directly to calculate the distances for other protons using the linear range of the NOE buildup curve:

$$r_{ab}^6 = \frac{I_{ref}}{I_a} r_{ref}^6 \tag{4.60}$$

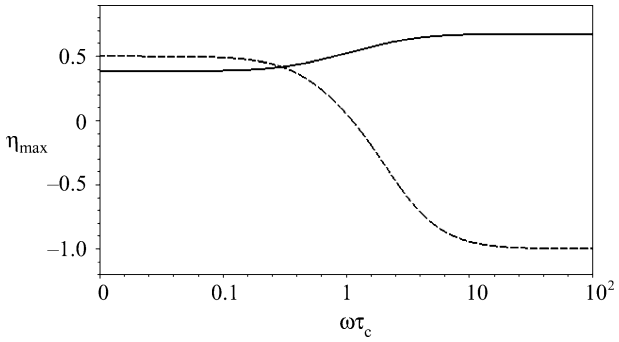

Fig. 4.22 NOE and ROE enhancement factor η_{max} as a function of $\omega\tau_c$. The steady-state NOE enhancement (*dashed line*) is close to zero when $\omega\tau_c \approx 1$, equals 0.5 for $\omega\tau_c \ll 1$ (extreme narrowing limit), and -1.0 for $\omega\tau_c \gg 1$ (spin diffusion limit). The ROE enhancement (*solid line*) is always positive in all regimes, and it is 0.38 for $\omega\tau_c \ll 1$ and 0.68 for $\omega\tau_c \gg 1$

The intensity ratio of each assigned cross peak is used to obtain the distance r_{ab}.

In addition to the spin diffusion effect, another limitation of the NOESY experiment is that the NOE enhancement is close to zero when $\omega\tau_c$ is approximately 1 (small and medium size molecules) as indicated in Fig. 4.22. To overcome these problems, the ROESY experiment has been developed. The pulse sequence of the ROESY experiment is similar to TOCSY although the cross peaks of a ROESY spectrum has an opposite phase to those in the TOCSY spectrum. The ROE enhancement is always positive in all regimes, and it is 0.38 for $\omega\tau_c \ll 1$ and 0.68 for $\omega\tau_c \gg 1$ (Fig. 4.22). The presence of TOCSY peaks in the ROESY spectrum will reduce the intensity of the ROESY cross-peaks. A typical solution is to use an inefficient spin lock scheme with an off-resonance B_1 to mismatch the Hartmann–Hahn matching condition that is required for the TOCSY experiment. Usually, the spin lock field strength for a ROESY experiment is in the order of 1–5 kHz and off-resonance from the carrier frequency by several kilohertz. Such a B_1 field is not sufficient for TOCSY isotropic mixing.

NOESY and ROESY data are collected in a phase sensitive mode in the F_1 dimension, for example, States-TPPI, with 512 increments that yield 256 complex points in the F_1 dimension. A mixing time in the range of 30–200 ms is usually used for NOESY, whereas the mixing time for the ROESY experiment is in the range of the rotating frame relaxation time $T_{1\rho}$, which can be longer than 500 ms for small molecules. Spin lock power for the ROESY is usually set to be less than 5 kHz and several kilohertz off-resonance from the carrier frequency. The data are acquired using 200 or more FIDs and linear prediction should be utilized to double data points for the F_1 dimension. The data are processed with a square sine-bell function shifted by 30–60° before Fourier transformation. The cross peaks of a NOESY spectrum have the same phase as the diagonal peaks, whereas the cross peaks of a ROESY spectrum have the opposite phase from the diagonal peaks.

Questions

1. For a 14.1 T magnet with a proton resonance frequency of 599.89836472 MHz at 0.0 ppm, what is the $^{13}C'$ 180° pulse length that gives a null at C^{α}?
2. For a 14.1 T magnet with a proton resonance frequency of 599.89836472 MHz at 0.0 ppm, what is the ^{13}C C' off-resonance 90° pulse length that does not disturb the on-resonance C^{α}?
3. When calibrating a shaped pulse (except a rectangular shaped pulse), which one of the two pulse parameters (pulse length and pulse power) is usually adjusted? And why?
4. What pulse length should be used for the GARP decoupling scheme if a 10 kHz decoupling field strength is desired for ^{13}C decoupling?
5. What is the difference between the watergate and water flip-back watergate sequences? Why does a water flip-back watergate generally yield superior water suppression for aqueous protein samples?
6. What happens to the spectrum if the receiver gain is set too high and how the gain is set for 2D and 3D experiments?
7. Why is a protein sample never span when acquiring data (water suppression, 2D and 3D data)?
8. Why must nonspinning shims be optimized first before gradient shimming on z shims?
9. Which nucleus do you shim when gradient shimming on a 90% H_2O/10% ^2H_2O sample? And explain why.
10. Why is there a splitting in ^2H spectrum of an alignment medium for dipolar measurement?
11. What is the modification of water flip-back made to the watergate solvent suppression sequence and for what purpose is the modification?
12. Why does a weighting function for resolution enhancement almost always decrease sensitivity of the spectrum?
13. Why is unshifted squared sine-bell function used for COSY data, but a 80–90°-shifted squared sine-bell function is used for 3D data?
14. Why is a 180° pulse used for ^1H pulse length calibration but 90° X pulse is used for heteronuclear decoupler pulse length calibration?
15. How many frequency axis or axes do 1D and 3D spectra have? Which parameter is present in any 2D and 3D experiment but not in any 1D experiment?
16. What are the typical ranges of gradient strengths used for suppressing water magnetization, perfecting a 180° pulse, and coherence selection?
17. Assuming that 32,000 DAC on an NMR spectrometer corresponds to the gradient strength of 70 Gcm^{-1}, what is the DAC value for a gradient of -30 Gcm^{-1}?

References

Abragam A (1961) Principles of nuclear magnetism. Clarendon Press, Oxford
Bain A (1984) Coherence levels and coherence pathways in NMR. A simple way to design phase cycling procedures. J Magn Reson 56:418–427
Barkhuijsen H, de Beer R, Bovée WMJ, van Ormindt D (1985) Retrieval of frequencies, amplitudes, damping factors, and phases from time-domain signals using a linear least-squares procedure. J Magn Reson 61:465–481
Bauer C, Freeman R, Frenkiel T, Keeler J, Shaka AJ (1984) Gaussian pulses. J Magn Reson 58:442–457
Baum J, Tycko R, Pines A (1985) Broadband and adiabatic inversion of a two-level system by phase-modulated pulses. Phys Rev A32:3435–3447
Bax A, Davis DG (1985a) Practical aspects of two-dimensional transverse NOE spectroscopy. J Magn Reson 63:207–213
Bax A, Davis DG (1985b) MLEV-17-based two-dimensional homonuclear magnetization transfer spectroscopy. J Magn Reson 65:355–360
Bodenhausen G, Kogler H, Ernst RR (1984) Selection of coherence-transfer pathways in NMR pulse experiments. J Magn Reson 58:370–388
Bothner-By AA, Stephens RL, Lee J, Warren CD, Jeanloz RW (1984) Structure determination of a tetrasaccharide: transient nuclear Overhauser effects in the rotating frame. J Am Chem Soc 106:811–813
Braunschweiler L, Ernst RR (1983) Coherence transfer by isotropic mixing: application to proton correlation spectroscopy. J Magn Reson 53:521–528
Connelly GP, Bai Y, Feng MF, Englander SW (1993) Isotope effects in peptide group hydrogen exchange. Proteins: Struct Funct Genet 17:87–92
Dykstra RW (1983) A broadband radiofrequency reflected-wave detector and its application to a nuclear magnetic resonance spectrometer. J Magn Reson 52:313–317
Emsley L, Bodenhausen G (1990) Gaussian pulse cascades: new analytical functions for rectangular selective inversion and in-phase excitation in NMR. Chem Phys Lett 165:469–476
Emsley L, Bodenhausen G (1989) Self-refocusing effect of 270° Gaussian pulses. applications to selective two-dimensional exchange spectroscopy. J Magn Reson 82:211–221
Emsley L (1994) Selective pulses and their applications to assignment and structure determination in nuclear magnetic resonance. Meth Enzymol 239:207–246
Ernst RR, Bodenhausen G, Wokaun A (1987) Principles of nuclear magnetic resonance in one and two dimensions. Oxford University Press, New York
Freeman R, Morris GA, Turner DL (1977) Proton-coupled carbon-13 J spectra in the presence of strong coupling. I. J Magn Reson 26:373–378
Friedrich J, Davies S, Freeman R (1987) Shaped selective pulses for coherence-transfer experiments. J Magn Reson 75:390–395
Geen H, Freeman R (1991) Band-selective radiofrequency pulses. J Magn Reson 93:93–141
Griesinger C, Ernest RR (1987) Frequency offset effects and their elimination in NMR rotating-frame cross-relaxation spectroscopy. J Magn Reson 75:261–271
Grzesiek S, Bax A (1993) The importance of not saturating water in protein NMR. Application to sensitivity enhancement and NOE measurements. J Am Chem Soc 115:12593–12594
Harris R, Becker ED, de Menezes SMC, Goodfellow R, and Granger P, NMR Nomenclature. Nuclear Spin Properties And Conventions For Chemical Shifts, Pure Appl. Chem., Vol. 73, pp. 1795–1818, 2001
Hartmann SR, Hahn EL (1962) Nuclear double resonance in the rotating frame. Phys Rev 128:2042–2053
Kay LE, Marion D, Bax A (1989) Practical aspects of 3D heteronuclear NMR of proteins. J Magn Reson 84:72–84
Keeler J, Clowes RT, Davis AL, Laue ED (1994) Pulsed-field gradients: theory and practice. Meth Enzymol 239:145–207

Kupče Ē (2001) Applications of adiabatic pulses in biomolecular nuclear magnetic resonance. Meth Enzymol 338:82–111
Kupče Ē, Freeman R (1995) Adiabatic Pulses for wideband inversion and broadband decoupling. J Magn Reson A115:273–276
Kupče Ē, Freeman R (1996) Optimized adiabatic pulses for wideband spin inversion. J Magn Reson A118:299–303
Marion D, Wuthrich K (1983) Application of phase sensitive two-dimensional correlated spectroscopy (COSY) for measurements of 1H-1H spin-spin coupling constants in proteins. Biochem Biophys Res Comm 113:967–974
Marion D, Ikura M, Bax A (1989a) Improved solvent suppression in one- and two-dimensional NMR spectra by convolution of time-domain data. J Magn Reson 84:425–430
Marion D, Ikura M, Tschudin R, Bax A (1989b) Rapid recording of 2D NMR spectra without phase cycling. Application to the study of hydrogen exchange in proteins. J Magn Reson 85:393–399
McCoy MA, Mueller L (1993) Selective decoupling. J Magn Reson A101:122–130
Norris D (2002) Adiabatic radiofrequency pulse forms in biomedical nuclear magnetic resonance. Concepts Magn Reson 14:89–101
Otting G, Widmer H, Wagner G, Wuthrich K (1986) Origin of τ_2 and τ_2 ridges in 2D NMR spectra and procedures for suppression. J Magn Reson 66:187–193
Piotto M, Saudek V, Sklenár V (1992) Gradient-tailored excitation for single-quantum NMR spectroscopy of aqueous solutions. J Biomol NMR 2:661–665
Plateau P, Guéron M (1982) Exchangeable proton NMR without base-line distorsion, using new strong-pulse sequences. J AM Chem Soc 104:7310–7311
Redfield AG, Kunz SD, Ralph EK (1975) Dynamic range in Fourier transform proton magnetic resonance. J Magn Reson 19:114–117
Rucker SP, Shaka AJ (1989) Broadband homonuclear cross polarization in 2D N.M.R. using DIPSI-2. Mol Phys 68:509–517
Shaka AJ, Lee CJ, Pines A (1988) Iterative schemes for bilinear operators; application to spin decoupling. J Magn Reson 77:274–293
Shaka AJ, Keeler J, Freeman R (1983) Evaluation of a new broadband decoupling sequence: WALTZ-16. J Magn Reson 53:313–340
Shaka AJ, Barker PB, Freeman R (1985) Computer-optimized decoupling scheme for wideband applications and low-level operation. J Magn Reson 64:547–552
States J, Haberkorn RA, Ruben DJ (1982) A two-dimensional nuclear overhauser experiment with pure absorption phase in four quadrants. J Magn Reson 48:286–292
Tannus A, Garwood M (1996) Improved performance of frequency-swept pulses using offset-independent adiabaticity. J Magn Reson A120:133–137
Xu P, Wu XL, Freeman R (1992) User-friendly selective pulses. J Magn Reson 99:308–322
Zhu G, Bax A (1990) Improved linear prediction for truncated signals of known phase. J Magn Reson 90:405–410